Swiss Journal of Palaeontology

RESEARCH

Open Access

A redescription of *Brouffia orientalis* Carroll & Baird, 1972 from the Upper Carboniferous of the Czech Republic and the status and affinities of protorothyridid amniotes

Jozef Klembara[1,5*], Marcello Ruta[2*], Jason Anderson[3], Taran Mayer[4], Miroslav Hain[5] and Daniel Valaška[6]

Abstract

The Upper Carboniferous protorothyridid amniote *Brouffia orientalis* from Czech Republic is redescribed. Photogrammetric scanning of the holotype and only known specimen yields considerable new information on the skull and postcranium of this tetrapod and allows us to amend previous morphological descriptions to a substantial degree. A virtual 3D model built from photogrammetry scan data is used as the basis for a new reconstruction of the skull in dorsal, lateral, and ventral aspects and the lower jaw in lateral aspect. We expand and refine the diagnosis of *Brouffia* and compare it with other protorothyridids. We discuss the affinities of this taxon by coding it in a recently published data matrix of early amniotes, which we subject to maximum parsimony and Bayesian fossilized birth–death analyses. *Brouffia* emerges as the sister taxon to *Coelostegus* in all analyses, but the position of these two taxa within amniotes varies. In a parsimony analysis with unweighted characters, the (*Brouffia* + *Coelostegus*) clade forms the sister group to Synapsida. In various experiments of character reweighting, that clade is placed crownward of Captorhinidae on the stem-group of Reptilia, but anticrownward of remaining protorothyridids. The latter constitute either a paraphyletic array relative to Diapsida or their monophyletic sister group. The Bayesian analysis retrieves (*Brouffia* + *Coelostegus*) as the most basal plesion on the stem-group of Reptilia.

Introduction

Among the earliest Reptilia (Laurenti, 1768) are seven key genera from Europe and North America that have played a fundamental role in our understanding of early amniote evolution (Tsuji & Müller, 2009). Six of those genera, all Middle Pennsylvanian in age, are monotypic, and include: *Brouffia* and *Coelostegus* from Nýřany (Czech Republic); *Hylonomus* and *Paleothyris*, respectively from Joggins and Florence, Nova Scotia (Canada); *Cephalerpeton* and *Anthracodromeus*, respectively from Mazon Creek, Illinois and Linton, Ohio (USA) (Carroll, 1969; Carroll & Baird, 1972). The seventh genus, *Protorothyris*, encompasses two species from the Early Permian of Texas and West Virginia (Clark & Carroll, 1973; Price, 1937; Romer, 1952). All seven genera have been assigned to the Family Protorothyrididae, generally (but not

Handling editor: Hans-Dieter Sues.

*Correspondence:
Jozef Klembara
jozef.klembara@uniba.sk
Marcello Ruta
mruta@lincoln.ac.uk
[1] Department of Ecology, Laboratory of Evolutionary Biology, Faculty of Natural Sciences, Comenius University in Bratislava, Bratislava, Slovakia
[2] Joseph Banks Laboratories, Department of Life Sciences, University of Lincoln, Lincoln, UK
[3] Faculty of Veterinary Medicine, University of Calgary, Calgary, AB, Canada
[4] Department of Comparative Biology and Experimental Medicine, University of Calgary, Calgary, AB, Canada
[5] Institute of Measurement Science, Slovak Academy of Sciences, Bratislava, Slovakia
[6] Scanstudio S.R.O., Šancová, 7961/11B Bratislava, Slovakia

unanimously) considered to represent a non-monophyletic assortment of early diverging, crown-group amniotes (Mann et al., 2019). No consensus has emerged on the intrinsic relationships and wider affinities of this group. Thus, whereas several authors have considered protorothyridids to be phylogenetically proximal to Diapsida (e.g., Ford & Benson, 2020; Müller & Reisz, 2006), others have placed them in a derived position along the stem-group of Amniota (e.g., Simões et al., 2022).

Only a few protorothyridids have been re-investigated since their original descriptions (e.g., *Cephalerpeton*; Mann et al., 2019; *Anthracodromeus*; Mann et al., 2021; *Coelostegus*; Klembara et al., 2023), and several require a comprehensive re-examination. Klembara et al. (2023) discussed protorothyridids in their revision of *Coelostegus prothales*, one of the least well-understood and phylogenetically least stable taxa within the group (e.g., Müller & Reisz, 2006), and provided a succinct (albeit provisional) account of similarities and differences in skull morphology between *Coelostegus* and other protorothyridid genera. Their phylogenetic analyses (parsimony, using Ford & Benson's, 2020 and Simões et al.,'s 2022 data matrices and uncalibrated Bayesian, using Ford & Benson's, 2020 data matrix) yielded different outcomes for the placement of *Coelostegus*. Depending upon the type of analysis, *Coelostegus* appeared either on the stem-group of Amniota or on the stem-group of Diapsida (sensu Ford & Benson, 2020) and, in the latter case, its position varied from basal (i.e., earliest diverging) to derived (i.e., most crownward) (Klembara et al., 2023).

The subject of the present work is the second protorothyridid from Nýřany, *Brouffia orientalis*. As in the case of *Coelostegus* and other amniotes and near-amniote tetrapods from this locality, *Brouffia* has a convoluted history (Carroll, 1970; Carroll & Baird, 1972). Thus, it was originally described by Brough & Brough (1967) as *Specimen I* under the hypodigm of the putative stem-group amniote *Gephyrostegus bohemicus* (see Klembara et al., 2014 for a historical account). Subsequently, Carroll (1970) recognized that *Specimen I* is taxonomically distinct from *G. bohemicus*. Carroll & Baird (1972) re-described *Specimen I* as a primitive amniote under the binomen *Brouffia orientalis* and placed it within the now obsolete Family Romeriidae. In their phylogenetic study of early reptiles, Müller & Reisz (2006) retrieved *Brouffia* in different positions in their parsimony and Bayesian analyses. Parsimony placed *Brouffia* as the most plesiomorphic taxon along the stem-group of Diapsida (represented by *Araeoscelis* and *Petrolacosaurus* in their analysis), followed by *Paleothyris*, *Hylonomus*, and a clade of (*Protorothyris*, *Anthracodromeus*, *Cephalerpeton*) in crownward succession. Their non-calibrated Bayesian analyses (under a variety of settings that permitted equal or unequal rates of character-state changes and included or excluded autapomorphies) invariably placed *Brouffia* as sister taxon to *Hylonomus*. In turn, the (*Brouffia* + *Hylonomus*) clade formed the sister group to (*Paleothyris* + Captorhinidae), while other protorothyridids (*Cephalerpeton* + (*Anthracodromeus* + *Paleothyris*)) joined Diapsida. At the time when our re-description of *Coelostegus* (Klembara et al., 2023) was submitted, we had not completed our re-assessment of *Brouffia*. Therefore, this taxon was not considered in our phylogenetic analysis.

Brough & Brough (1967) illustrated the skull of *Brouffia* in dorsal and ventral aspects. Our results indicate that their drawings of several cranial bones are reasonably accurate, and that many—but not all—elements were correctly identified. For example, the lateral lappet of the parietal was considered by them to represent an intertemporal, as already noted by Carroll (1970). In contrast, Carroll & Baird (1972) did not provide an exhaustive description of all preserved cranial elements, many of which were not illustrated (e.g., bones in the pre-orbital region). We have not been able to ascertain possible reasons for the discrepancies between Brough & Brough's (1967) and Carroll & Baird's (1972) accounts. This is puzzling because Carroll & Baird (1972) clearly acknowledged the Broughs' permission to examine Nýřany specimens in their possession and to produce new latex casts. In addition, they stated that the skull of *Brouffia* had been redrawn from original—presumably, Brough & Brough's (1967)—latex casts. Examination of Carroll's (1970) work on *Gephyrostegus bohemicus* did not cast further light on this issue. In addition, the illustrations of the cranial anatomy of *Brouffia* (then, *Specimen I*) in that work are the same as those reproduced in Carroll & Baird (1972). Carroll & Baird (1972) compared *Brouffia* to the nearly coeval *Paleothyris acadiana* from the uppermost Westphalian of Nova Scotia (see Carroll, 1969), and offered a cautionary note about the taxonomic distinctiveness of *Brouffia* at genus level, as the only known specimen may belong to an immature individual. We return to this point in our Discussion.

Brouffia is known from a single specimen preserved as an external mould on part and counterpart slabs. As in Klembara et al., (2023), we used photogrammetric scanning to obtain a virtual 3D model of its skull. Photogrammetry allowed us to amend previous descriptions of the cranial anatomy of *Brouffia* and to glean substantial new data. Additional information on the postcranium of this taxon also became available during our investigation.

The aims of the present paper are (1) to redescribe the cranial and postcranial anatomy of *Brouffia orientalis* using high-fidelity latex casts and photogrammetric

3D scanning; (2) to provide an amended and expanded diagnosis of this taxon; (3) to supply a new reconstruction of its skull and lower jaw; (4) to assess its phylogenetic position; (5) to re-evaluate anatomical evidence in support of the taxonomic separation between *Brouffia* and *Paleothyris*; (6) to draw a compendium of key cranial traits that differentiate *Brouffia* from other protorothyridids; (7) to provide a brief discussion of the possible lifestyle of *Brouffia*, based upon a quantitative treatment of its manus proportions.

Material and methods

Specimen preservation

Both part and counterpart slabs reveal the impressions of the ventral and dorsal surfaces of an articulated and lightly ossified skeleton (Figs. 1, 2, 3, 4). Diagenetic flattening has resulted, *inter alia*, in a disrupted skull roof. The left fore- and hindlimbs and most of the tail are missing. A complete, right forelimb and much of the right hindlimb are preserved. The specimen is about 150 mm long from the anterior extremity of the skull to the sacrum.

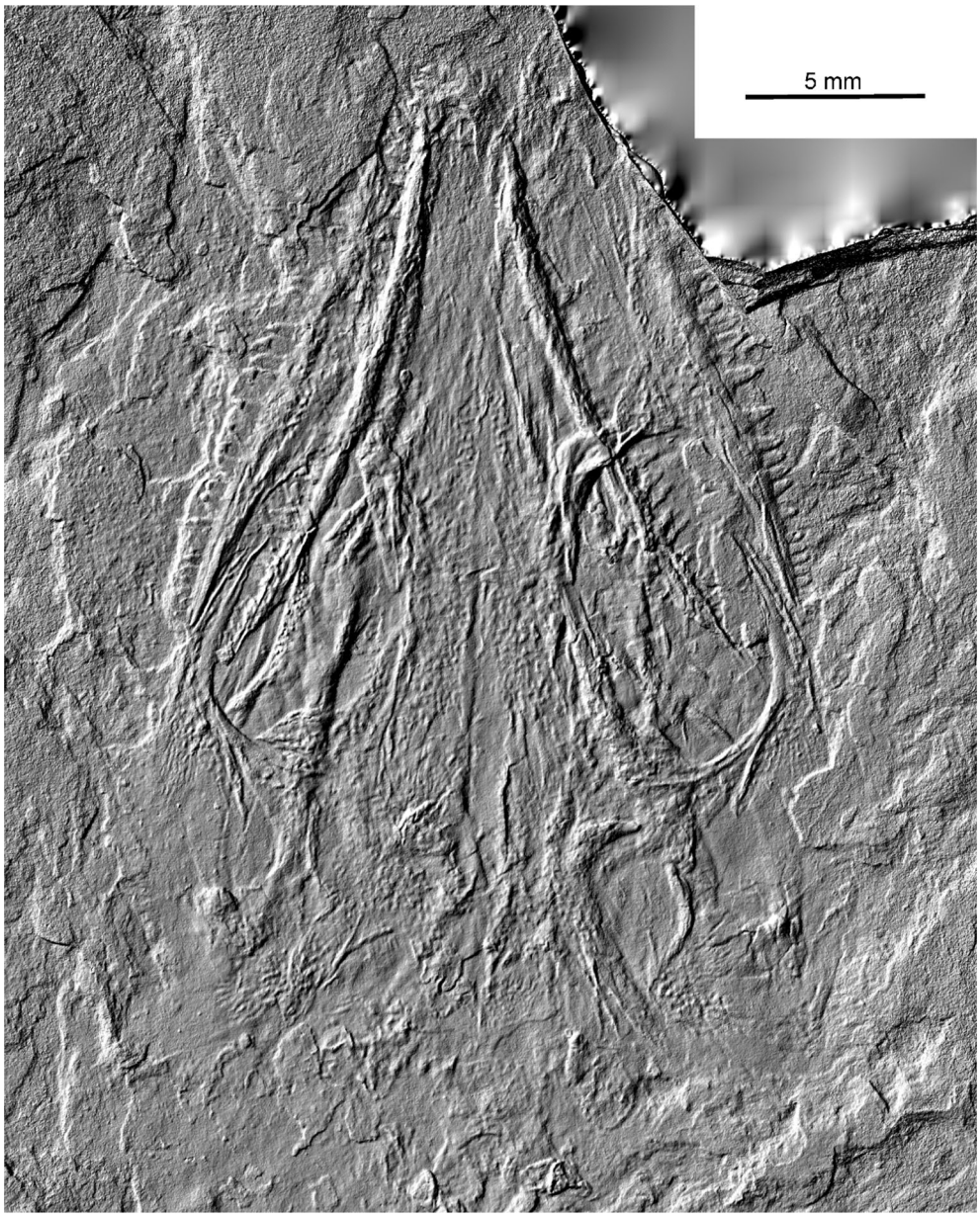

Fig. 1 *Brouffia orientalis* Carroll & Baird, 1972. Virtual 3D model of the skull in dorsal view

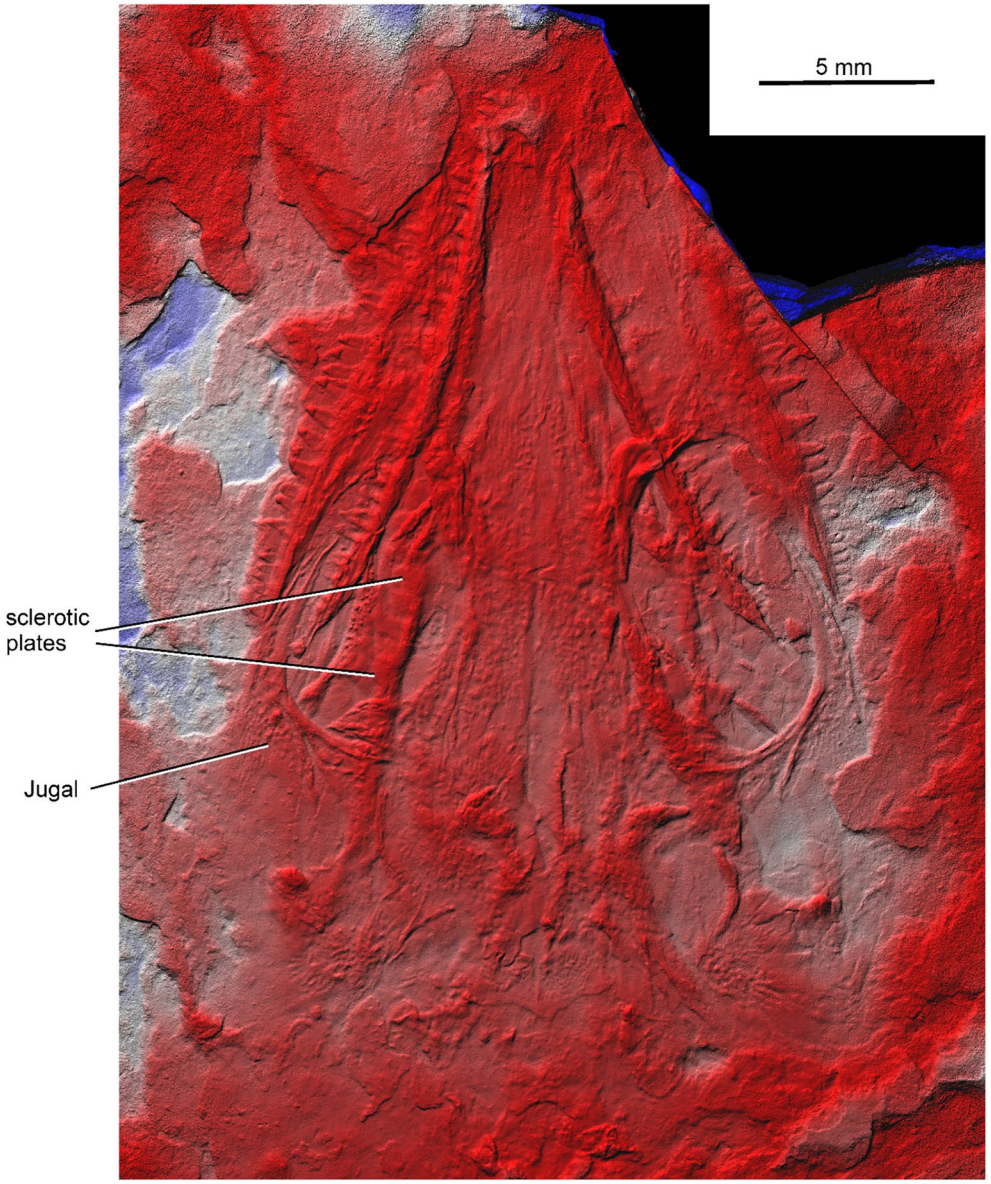

Fig. 2 *Brouffia orientalis* Carroll & Baird, 1972. Colour scale digital elevation model of the skull in dorsal view

The skull roof bones are thin, as detailed by Brough & Brough (1967). As a result, the profiles of the lower jaws are visible in dorsal view (Figs. 1, 2). In ventral view, the left and right lower jaws overlap the lateralmost portions of the skull (Figs. 3, 4). Despite a certain degree of disruption, however, the impressions of several skull roof bones reveal considerable detail. In several cases, their outlines can be discerned by changing the angle of illumination. As in our work on *Coelostegus* (Klembara et al., 2023), we have superimposed transparent colours over the images to highlight the extent and orientation of various skull roof elements.

The skull reconstruction was facilitated by the production of an enlarged wax-plasticine model. Each skull bone was measured and modelled at ten times natural size. The modelled bones were assembled in anatomical orientation and held together in place with flat metal bars.

Photogrammetric 3D scanning

Photogrammetric 3D scanning techniques were detailed by Klembara et al., (2023). They are succinctly presented in Supplementary Information (Additional file 1).

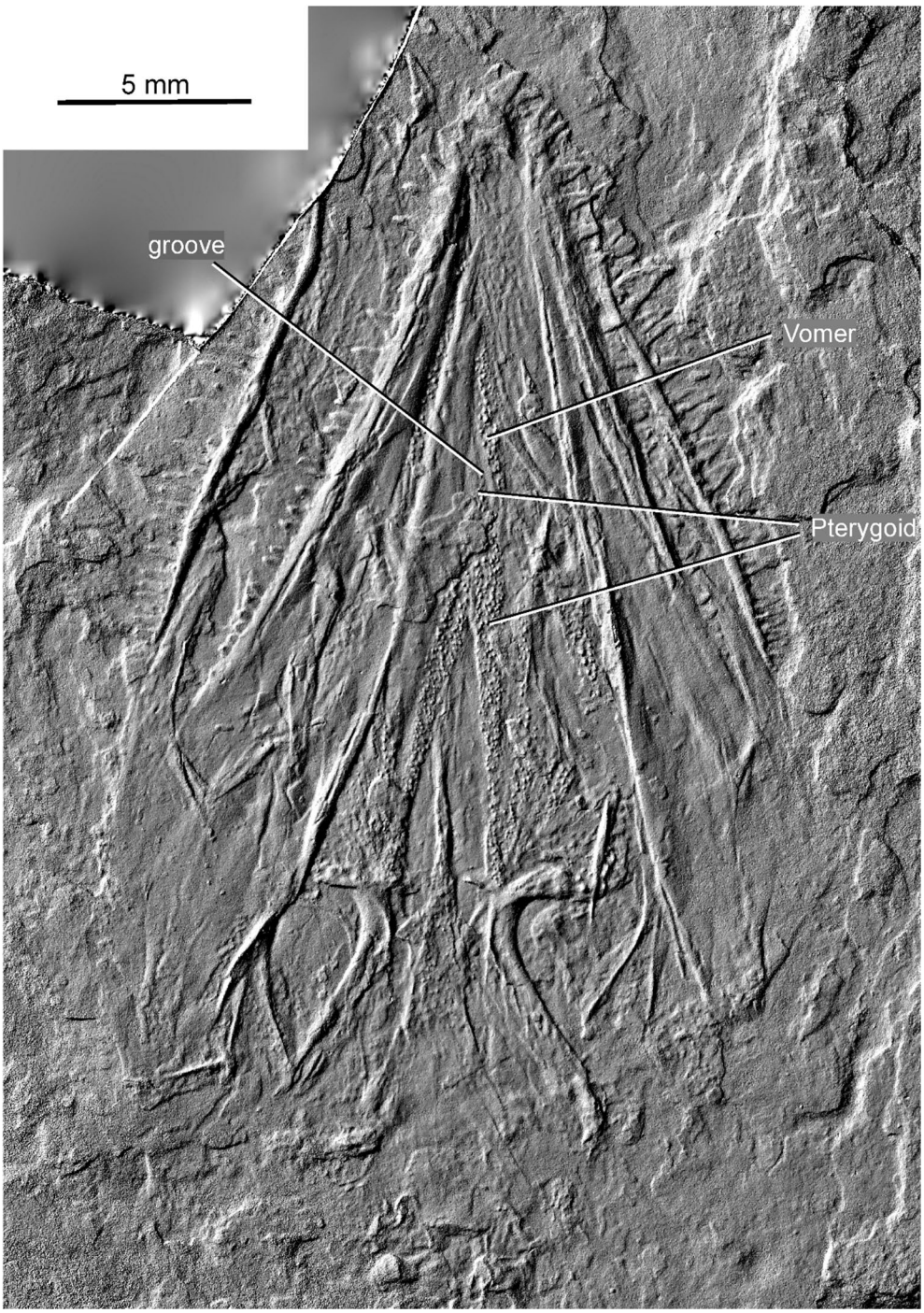

Fig. 3 *Brouffia orientalis* Carroll & Baird, 1972. Virtual 3D model of the skull in ventral view

Morphometric characterisation of manus proportions

The right manus of the only known specimen of *Brouffia* reveals considerable morphological information. Its peculiar combination of traits prompted a brief consideration of the possible lifestyle of this tetrapod. To this end, we added the manus measurements for *Brouffia* to the tetrapod dataset in Mann et al., (2021), an elaboration of a previous dataset built by Fröbisch & Reisz (1999). For analytical and statistical procedures, see Supplementary Information (Additional file 1).

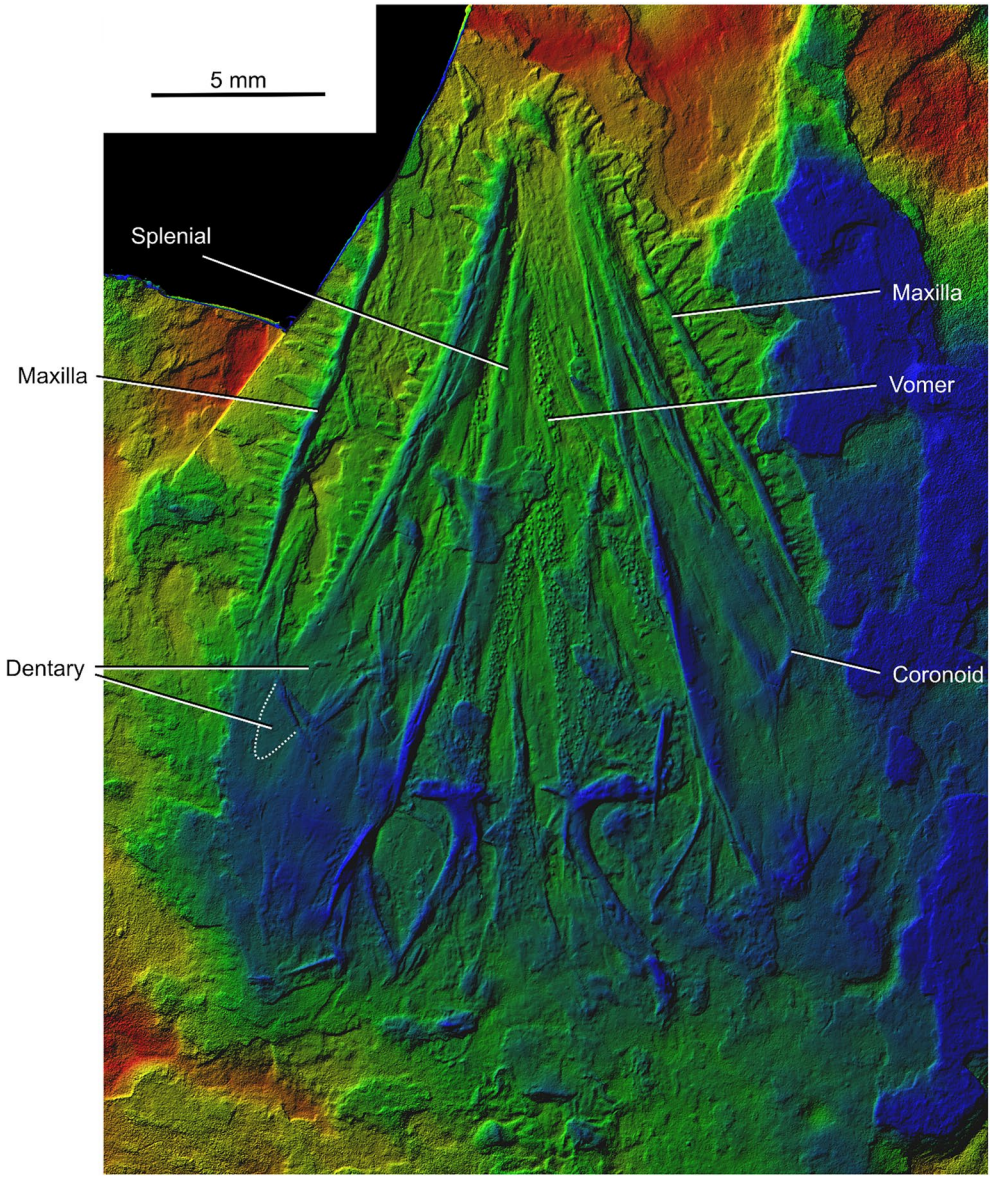

Fig. 4 *Brouffia orientalis* Carroll & Baird, 1972. Colour scale digital elevation model of the skull in ventral view. Colours in this elevation model are in reverse order relative to colour scale in Fig. 2

Phylogenetic analyses

In their re-investigation of *Coelostegus*, Klembara et al., (2023) used two recently published data matrices of early amniotes to investigate its affinities (Ford & Benson, 2020; Simões et al., 2022). While it would be appropriate to adopt a comparable approach here, we decided to code *Brouffia* into the matrix of Ford & Benson (2020) only, as the processing of the Simões et al., (2022) matrix proved to be extremely time consuming. As part of our research efforts to disentangle areas of conflict in early amniote phylogeny, we are in the process of collating an all-encompassing dataset of cladistic characters from those and other recent studies, and we acknowledge work by other research teams in this area. For these reasons, our phylogenetic treatment of *Brouffia* ought to be regarded as provisional.

We coded *Brouffia* in Klembara et al.,'s (2023) slightly modified version of Ford & Benson's (2020) data matrix (Supplementary Information, Additional file 2). Tree searches under maximum parsimony used three regimes of character weighting, i.e., equal weighting, simple re-weighting, and implied weighting. In addition, we performed a Bayesian fossilized birth–death (FBD) analysis (e.g., Gavryushkina et al., 2014; Heath et al., 2014; Stadler,

2010; Zhang et al., 2016), after adapting Ford & Benson's (2020) template script to accommodate *Brouffia* and *Coelostegus* (Supplementary Information, Additional file 3).

All parsimony analyses were run in PAUP* v. 4.0a.169 (Swofford, 1998) and utilised identical search settings to those expounded in Klembara et al., (2023). Firstly, we searched for the most parsimonious trees with all characters having equal unit weight. These searches employed tree bisection-reconnection as the preferred branch-swapping algorithm and 5×10^4 random stepwise sequences of taxon addition. Tree branches were collapsed if the minimum length of any branch was zero ("amb-" option). We retained one tree in memory at each step during this initial stage of the tree searches. Subsequently, all trees saved from this stage were input into a new round of tree branch swappings, this time with the option of saving multiple trees. As a final step, those trees were subjected to ten successive branch swapping iterations. Neither additional nor shorter trees were obtained after these iterations. Secondly, characters were re-weighted using the maximum values of their rescaled consistency indexes obtained in the initial analysis. Thirdly, we used implied weighting (Goloboff, 1993), with a value of 12 for the constant of concavity *K* (see Goloboff et al., 2018). If parsimony analyses resulted in multiple equally parsimonious trees, we summarized the conflicting topologies using a strict consensus. Node support in the equal-weights analysis was quantified through bootstrapping (Felsenstein, 1985) and jackknifing (Farris et al., 1996). With both methods, we employed the fast stepwise addition option, with 10^5 replicates of character resampling and a threshold of 50% character deletion for jackknifing. The bootstrap and jackknife majority-rule consensus topologies retained only groups with a frequency equal to or greater than 50%.

The Bayesian fossilized birth–death (FBD) analysis (5×10^7 generations) was performed in MrBayes v. 3.2.6 (Ronquist & Huelsenbeck, 2003). We visualized the FBD results in Figtree v. 1.4.4, available at: http://tree.bio.ed.ac.uk/software/figtree/. The FBD settings used by Ford & Benson (2020) were left unmodified. Thus, *Gephyrostegus* and *Seymouria* formed successive outgroups, in that order, to all other taxa. The groupings [*Seymouria* + higher taxa] and [higher taxa] were both constrained to be monophyletic. We specified a gamma model for rates (i.e., character-state changes are allowed to differ across the characters), a relaxed clock model conforming to an independent gamma rate (i.e., each branch of the phylogeny is permitted to experience a rate of evolution that does not depend upon the rates of adjacent branches), a variable type of character coding (i.e., neither constant nor uninformative characters are scored in the matrix), and an exponential parameter for the variance of the gamma distribution from which branch lengths are drawn. All taxa were assumed to be terminals (tips) and were sampled at random. We employed default prior values for the speciation, extinction, and sampling rates (Ronquist & Huelsenbeck, 2003). For exemplary explanations of these and other settings, see Müller & Reisz (2006), Ford & Benson (2020), and Simões et al., (2020).

Systematic paleontology

Tetrapoda Jaekel, 1909

Reptilia Laurenti, 1768 (phylogenetic definition sensu Modesto & Anderson, 2004).

Brouffia Carroll & Baird, 1972

Generic diagnosis: As for the only species, *Brouffia orientalis* Carroll & Baird, 1972

Type Species: *Brouffia orientalis* Carroll & Baird, 1972

***Brouffia orientalis* Carroll & Baird,** 1972

Figures 1, 2, 3, 4, 5, 6, 7, 8, 9, 10, 11, 12, 13, 14, 15.

Gephyrostegus bohemicus Jaekel, 1902; Brough & Brough, 1967:147–158, specimen I, figs. 2A, B, 4, 5A, 6B, 7B, 8B, 10A, B.

Brouffia orientalis Carroll & Baird, 1972:337–341, figs. 6, 11E.

Holotype

Part and counterpart blocks: M 4908a (formerly ČGH III B.21.C.587), dorsal aspect; M 4908b (formerly MP 451), ventral aspect (see Brough & Brough, 1967); National Museum, Prague, Czech Republic (Figs. 1, 2, 3, 4, 5, 6, 7, 8, 9, 10, 11, 12).

Locality and horizon

Nýřany 'Gaskohle', Nýřany Colliery, south-west of Plzeň, Czech Republic; apex of Lower Grey Beds, Plzeň-Manětín Basin; Upper Westphalian D (Asturian), Moscovian, Late Carboniferous (Middle Pennsylvanian) (see Klembara et al., 2014).

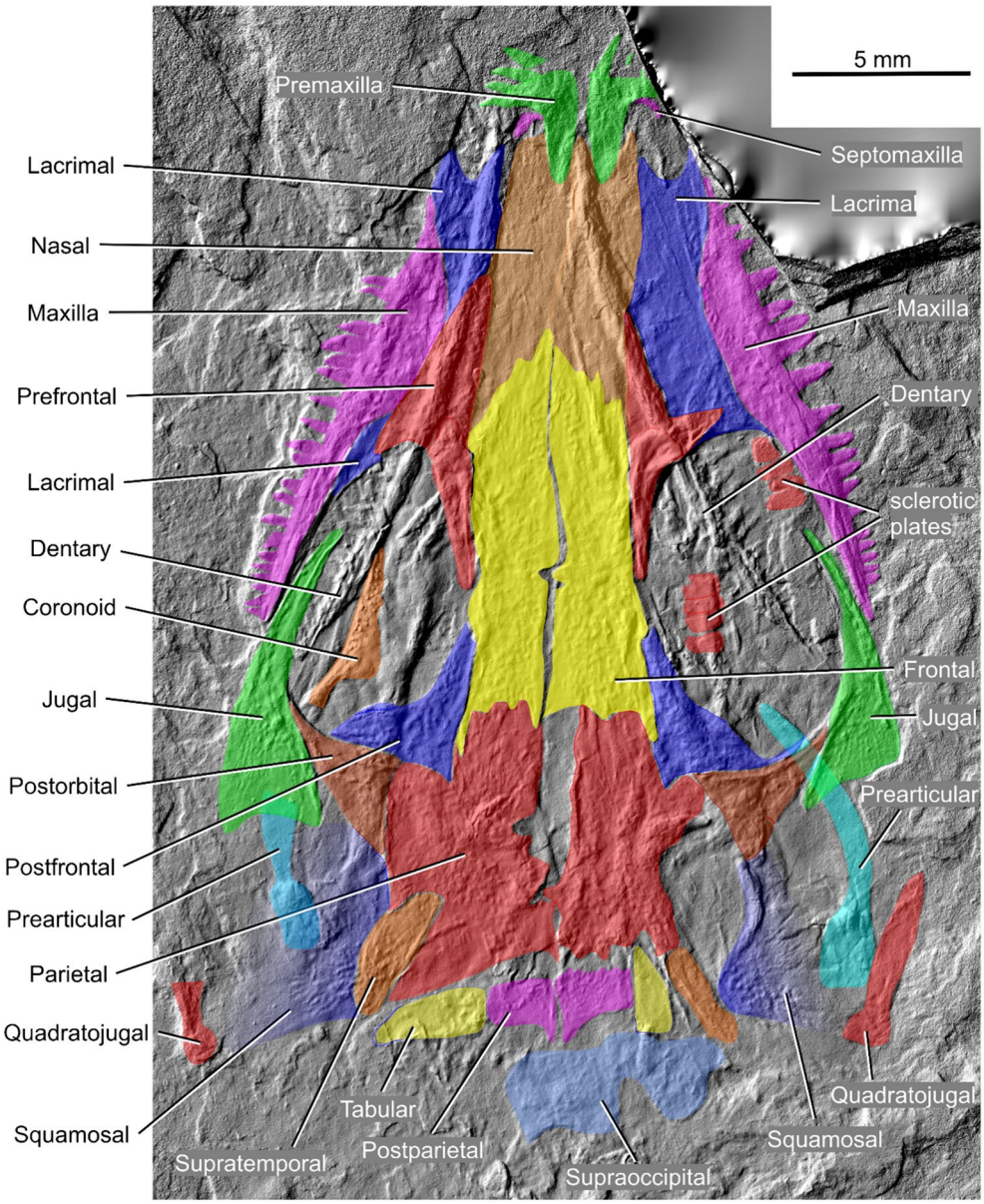

Fig. 5 *Brouffia orientalis* Carroll & Baird, 1972. Virtual 3D model of skull in dorsal view with individual bones in colour (cf. Figures 1, 2)

Amended diagnosis

In the following diagnosis, we focus on the principal characters that distinguish *Brouffia* from other protorothyridid genera. Additional anatomical differences among these genera are presented in the Discussion. We have not provided an exhaustive list of diagnostic features in *Brouffia*, because the polarity of several characters near the roots of crown-group Amniota is uncertain. This issue is compounded by the fact that the most recent, overarching analyses of early amniote phylogeny have yielded irreconcilable results for the intrinsic and extrinsic relationships of various clades.

Characters separating Brouffia from other protorothyridids: dermal skull roof sculpture consisting of clusters of tubercles of varying shape and size and accompanied by radiating ridges and grooves; dorsomedial surface of coronoid with extensive patch of densely arranged denticles; central portion of interclavicle plate covered in pebble-like, tubercular sculpture.

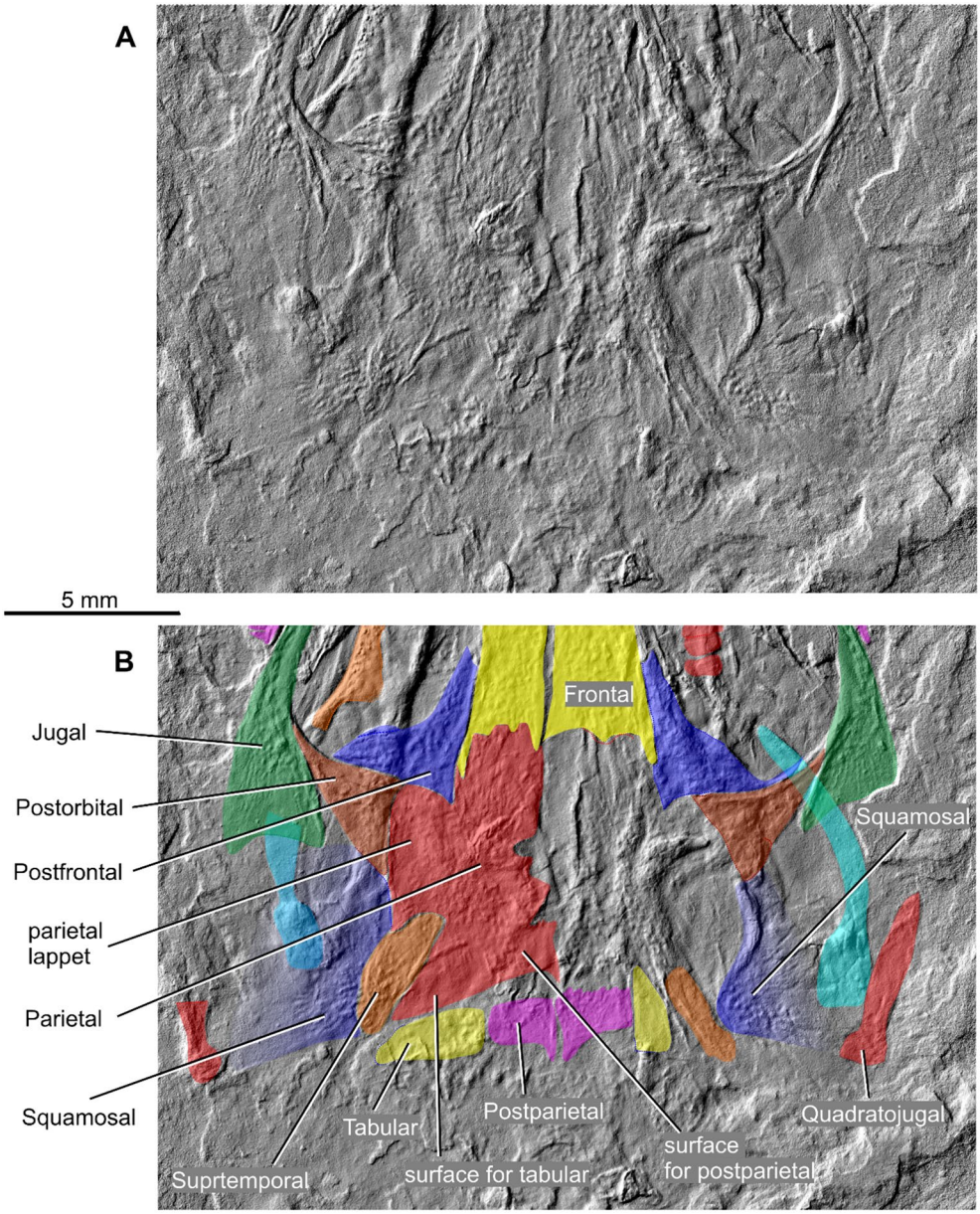

Fig. 6 *Brouffia orientalis* Carroll & Baird, 1972. **A** Virtual 3D model of posterior half of the skull in dorsal view. **B** The same portion of the skull with individual bones in colour

Main characters separating Brouffia from Paleothyris acadiana: three vs. two rows of palatal denticles; absence vs. presence of denticle patch on pterygoid transverse flange.

Main characters separating Brouffia from Coelostegus prothales: shallow vs. deep embayment of posterior margin of parietal; posterolateral process of frontal sturdy, finger-like, and blunt at its posterior extremity vs. narrow, elongate, and acuminate; anterior margin of supratemporal anterior vs. posterior to parietal posterior margin; larger number of maxillary teeth (~ 35 vs. ~ 24); single vs. multiple caniniform maxillary teeth.

Main characters separating Brouffia from Protorothyris archeri and P. morani: subelliptical vs. sliver-like supratemporal, with length greater than vs. smaller than greatest width of each of tabular and postparietal; absence vs. presence of conspicuous, posteromedial acuminate process on parietal posterior margin; absence vs. presence of transverse row of teeth on pterygoid flange.

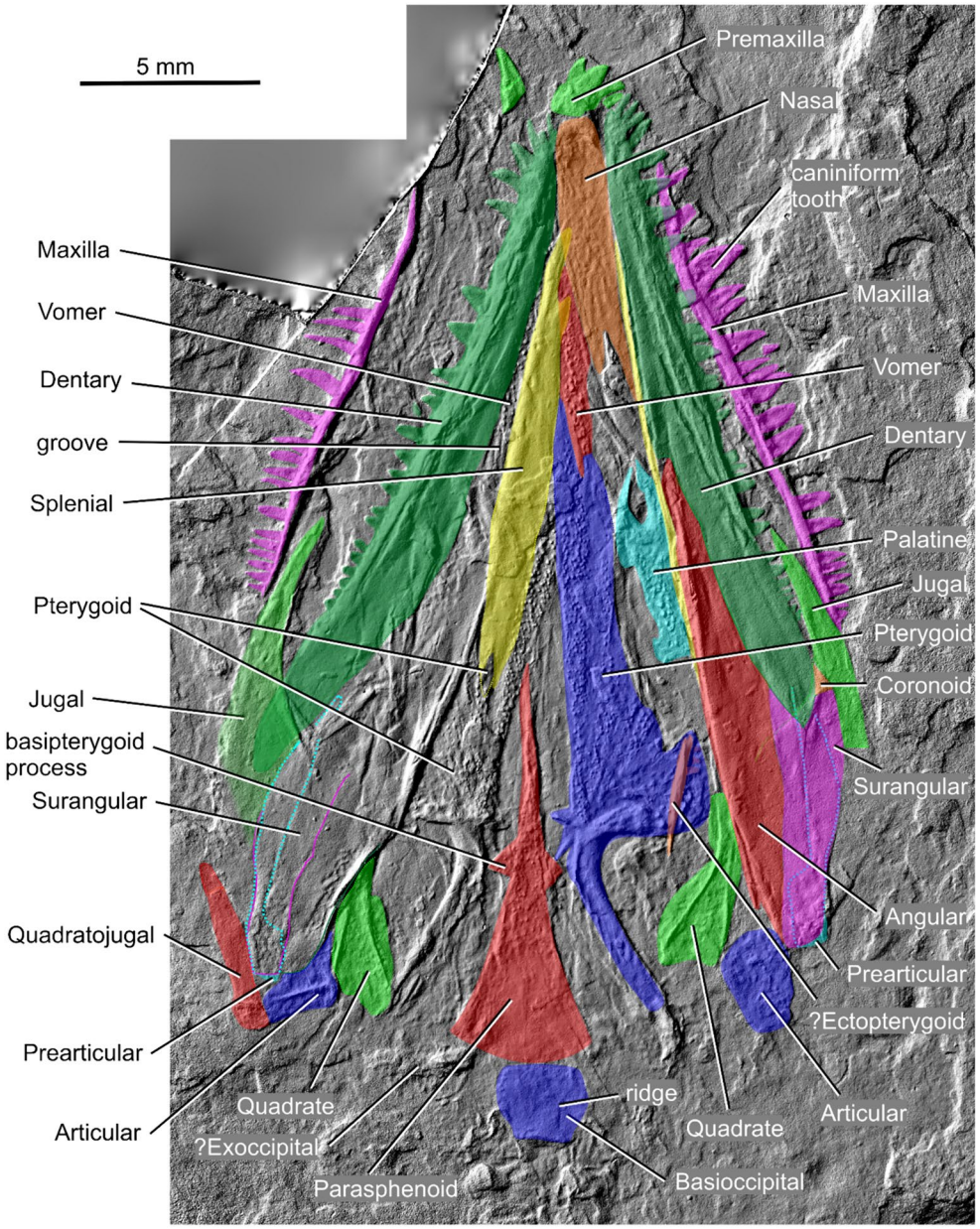

Fig. 7 *Brouffia orientalis* Carroll & Baird, 1972. Virtual 3D model of the skull in ventral view with individual bones in colour (cf. Figures 3, 4)

Main characters separating Brouffia from Cephalerpeton ventriarmatum: small vs. large upper marginal teeth; absence vs. presence of strong interdigitation at rearmost end of prefrontal-lacrimal suture (also in *Protorothyris archeri*).

Characters denoting immaturity: scapula and coracoid separately ossified; vertebral centra separate from neural arches; left and right halves of neural arches not co-ossified; humerus without well-developed processes.

Plesiomorphic characters in the context of crown-group amniotes: slightly raised patch of denticles on parasphenoid shaped like isosceles triangle; small exposure of coronoid in lateral view; single, posterior process of ilium; phalangeal counts of 2-3-4-5?-3.

Characters of uncertain polarity: nasal-frontal suture oblique; triangular posterior process of postfrontal accommodated by small, deep incisure between corpus and lappet of parietal, extending slightly posterior to transverse

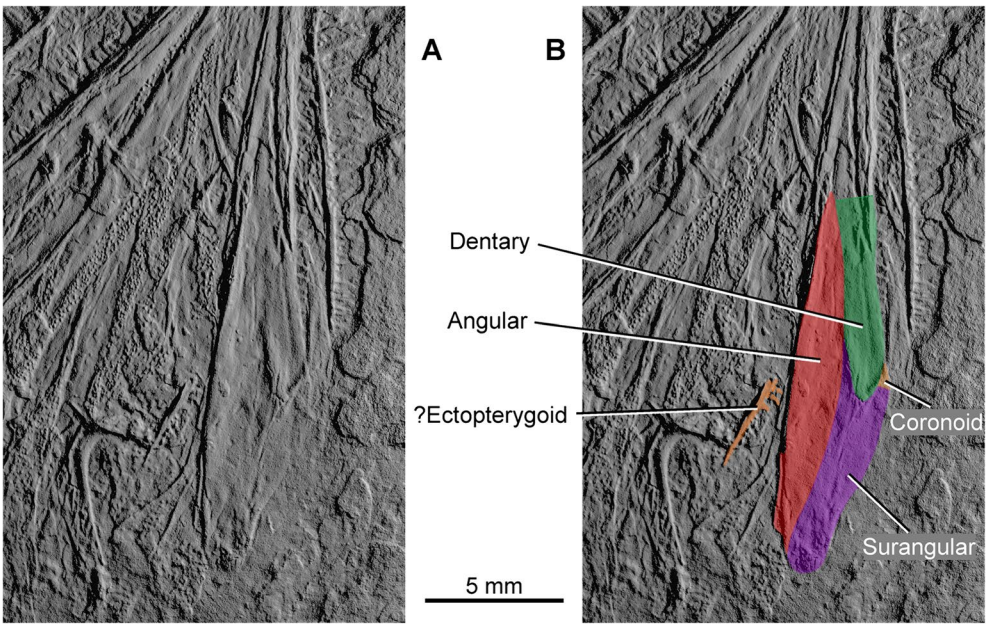

Fig. 8 *Brouffia orientalis* Carroll & Baird, 1972. **A** Virtual 3D model of part of the skull in ventral view and lower jaw in external view, and with individual bones in colour (**B**)

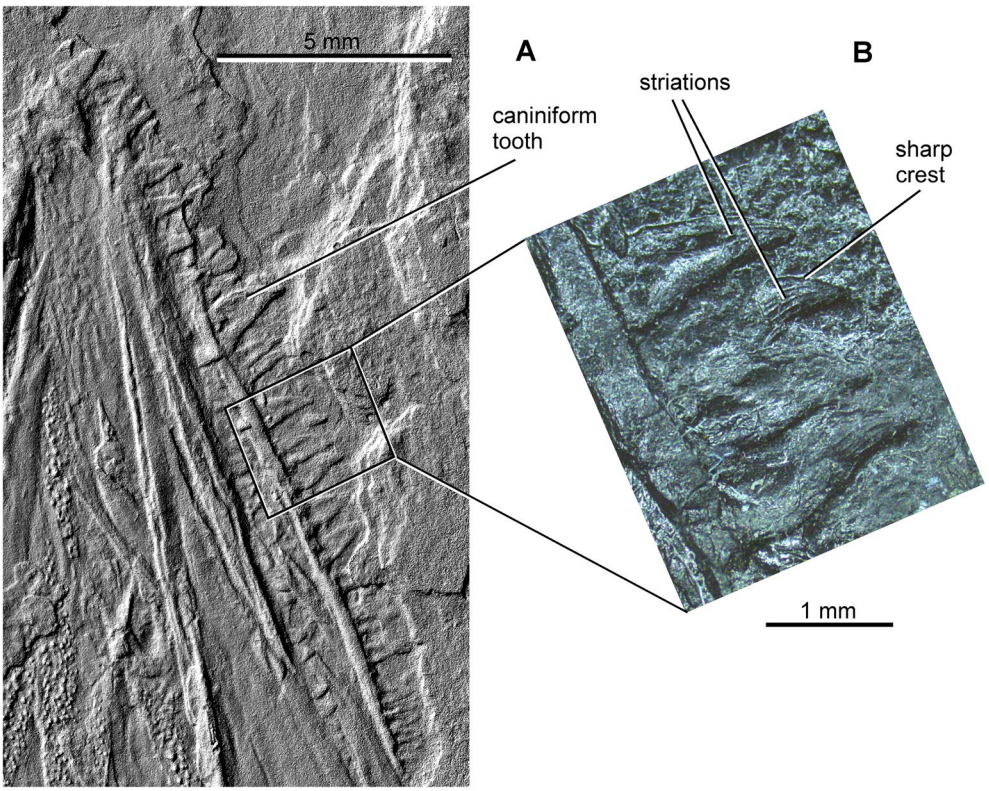

Fig. 9 *Brouffia orientalis* Carroll & Baird, 1972. **A** Virtual 3D model of part of the skull in ventral view and lower jaw in external view. **B** Part of the left maxilla with teeth in internal view

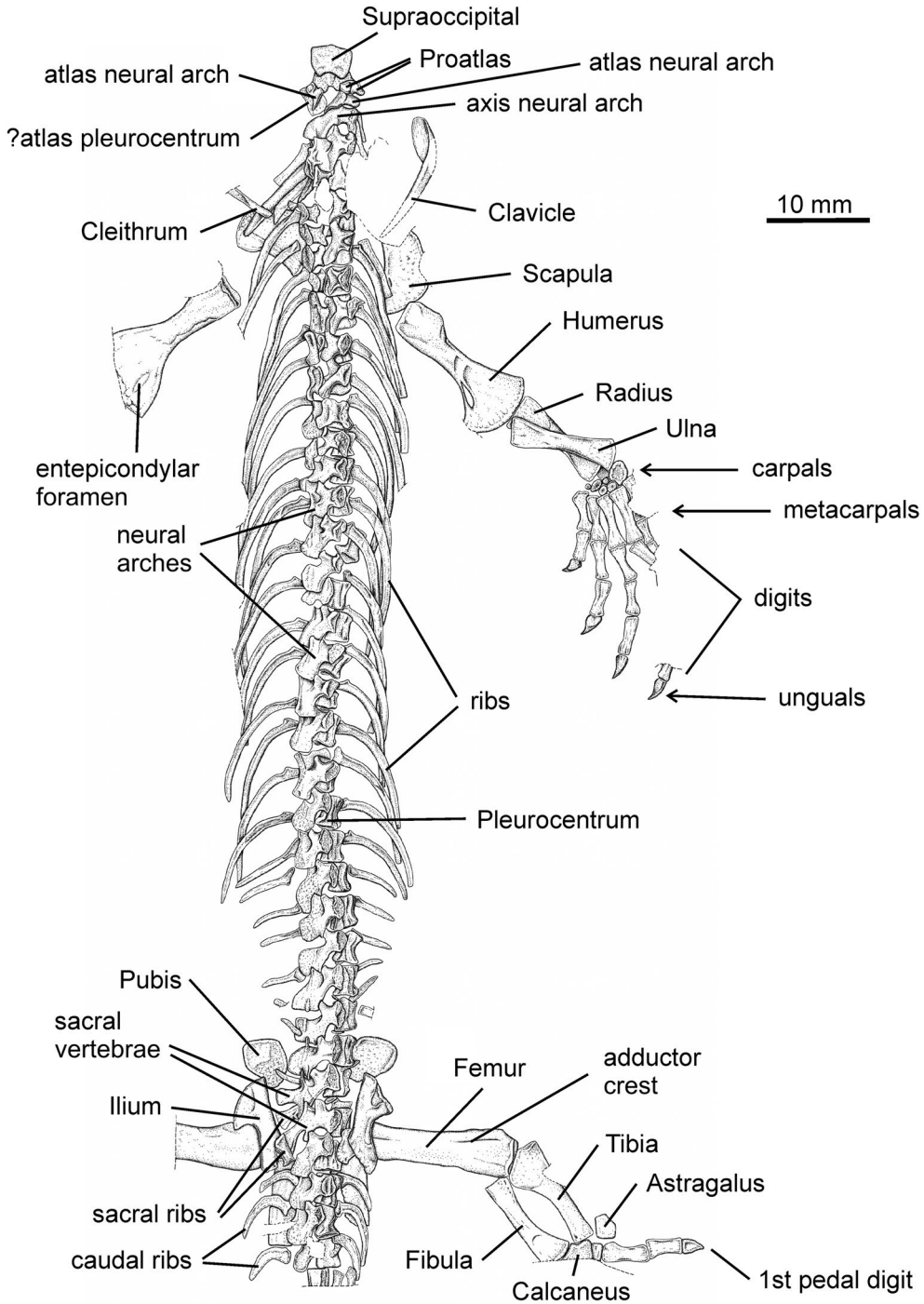

Fig. 10 *Brouffia orientalis* Carroll & Baird, 1972. Drawing of the postcranial skeleton in dorsal view

level of anterolateral corner of lappet; postorbital-parietal suture marginally longer than squamosal-parietal suture; triple sutural joint between frontal, parietal, and postfrontal occurring anterior to mid-length of pre-pineal portion of inter-parietal suture; carpals ossified; robust unguals on manus digits I and II; 31 presacral vertebrae.

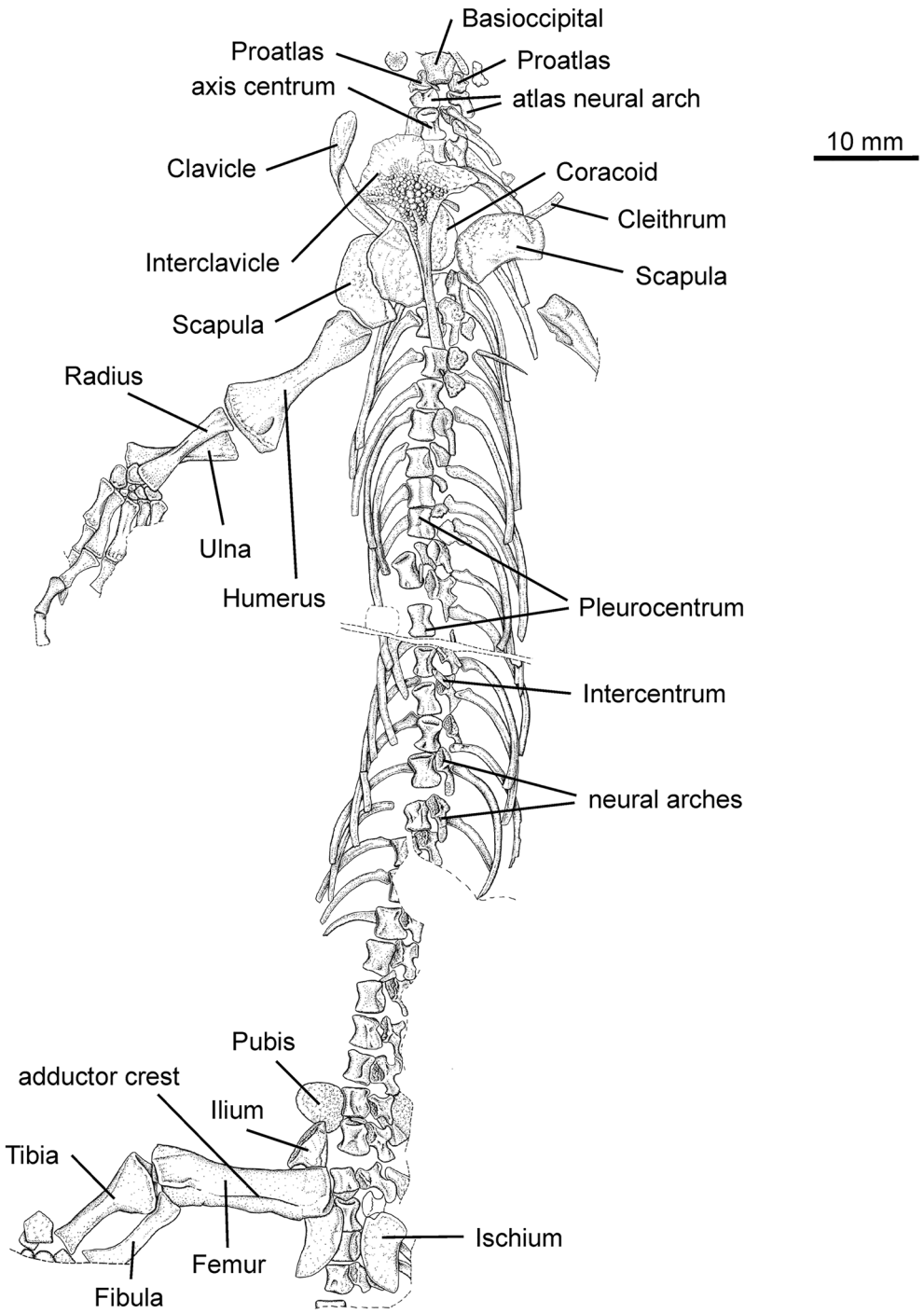

Fig. 11 *Brouffia orientalis* Carroll & Baird, 1972. Drawing of the postcranial skeleton in ventral view

Description

Skull roof

Most bones are well preserved, especially in the posterior part of the skull roof (Figs. 1, 2, 5, 6). In the snout region, several sutures are either disrupted or not recognizable as the lower jaws protrude against the ventral side of the overlying bones. Most skull roof bones feature a pronounced dermal sculpture of irregular tubercles of various sizes and radiating ridges and grooves. Generally, a few tubercles appear larger and more elongate than the rest. Smaller tubercles tend to be subcircular in outline. On several bones, isolated patches of tubercles

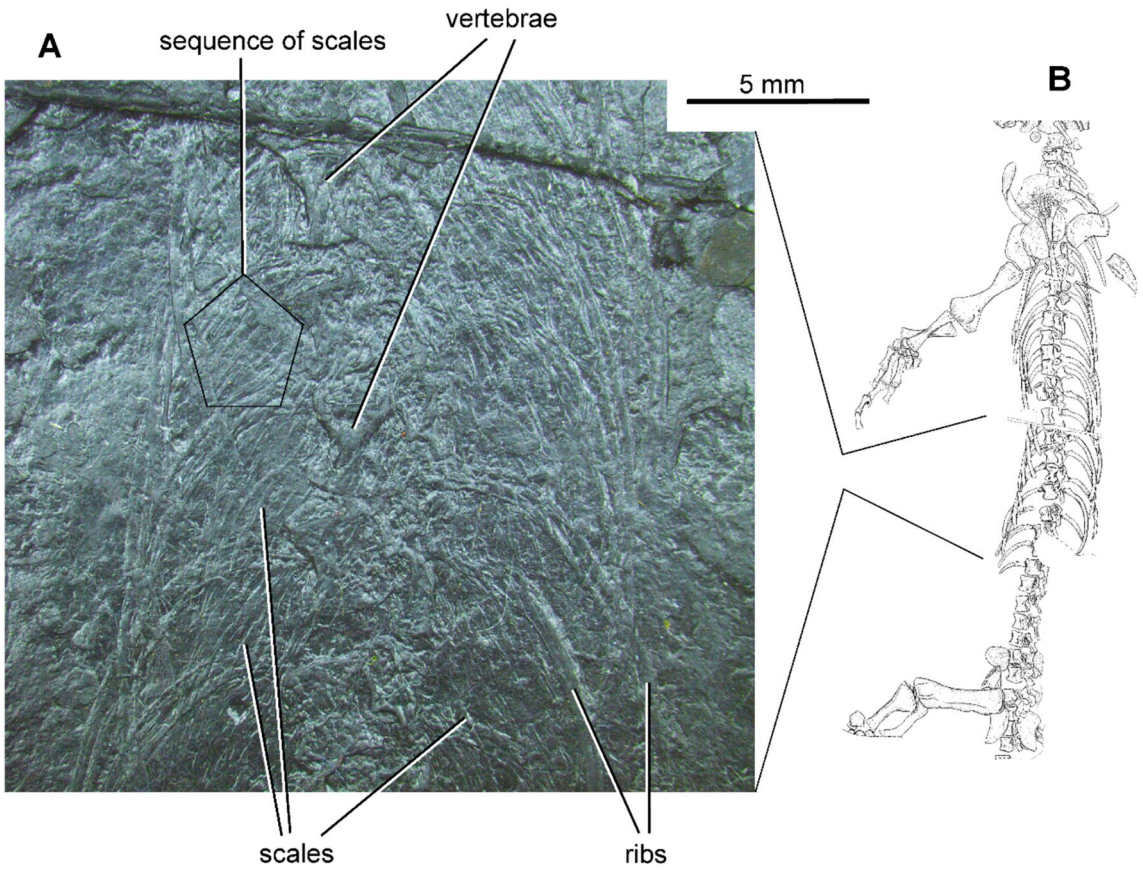

Fig.12 *Brouffia orientalis* Carroll & Baird, 1972. **A** Photograph of ventral scales from the middle portion of the postcranial skeleton in ventral view (**B**)

are visible more peripherally (e.g., nasals; frontals; lacrimals; prefrontals; parietals; postparietals). The portion of the external bone surface where the tubercles appear more densely arranged usually marks the position of the ossification centres. Grooves extend peripherally from these centres and cover most of the external bone surface. These grooves vary in density and depth across different regions of the skull. A system of alternating ridges and grooves is mainly observed on the anterior portions of the frontals and parietals. Changes in dermal sculpture are best conveyed with reference to Figs. 1, 2, 5, 6.

Both premaxillae are visible (Figs. 1, 5). The nasal ramus, which is well preserved on the right premaxilla, gradually narrows posterodorsally and terminates in a smooth, rounded extremity. The lateralmost portions of the ventral rami are not preserved on either premaxilla, although such rami appear to taper smoothly in a posterior direction. The external surface of the premaxilla, at the junction between the nasal ramus and the ventral ramus, shows a small cluster of tubercles separated by irregular depressions (Figs. 5).

On each side of the snout, in the region delimited by the nasals and the ventral rami of the premaxillae (corresponding to the external naris), a gently arcuate plate may represent a fragment of the septomaxilla (Figs. 1, 2, 5), but no morphological details are discernible. The left, wider fragment is L-shaped, with a posteriorly directed—as preserved—semielliptical extremity and a medially directed, subrectangular anterior process, and sits in the middle of the left external naris. The narrower, right fragment is approximately crescent-shaped. It is close to the anterior margin of the right external naris, adjacent to the ventral ramus of the right premaxilla.

Both nasals are preserved. Although their lateral margins are not entirely visible, their overall shape can be determined reasonably accurately based upon the shape of surrounding elements (Figs. 1, 2, 3, 4, 5). Each nasal is elongate and subrectangular, and slightly shorter than the frontal. Its anterolateral margin contributes to the posterodorsal margin of the external naris. Its anteromedial portion forms a stout subtrapezoidal process articulated with the nasal ramus of the premaxilla. Anterior and posterior to the triple sutural joints between the nasals, the lacrimals, and the prefrontals, the width of the nasals decreases imperceptibly. The nasal-frontal sutures are markedly oblique and, as a result, the frontals appear

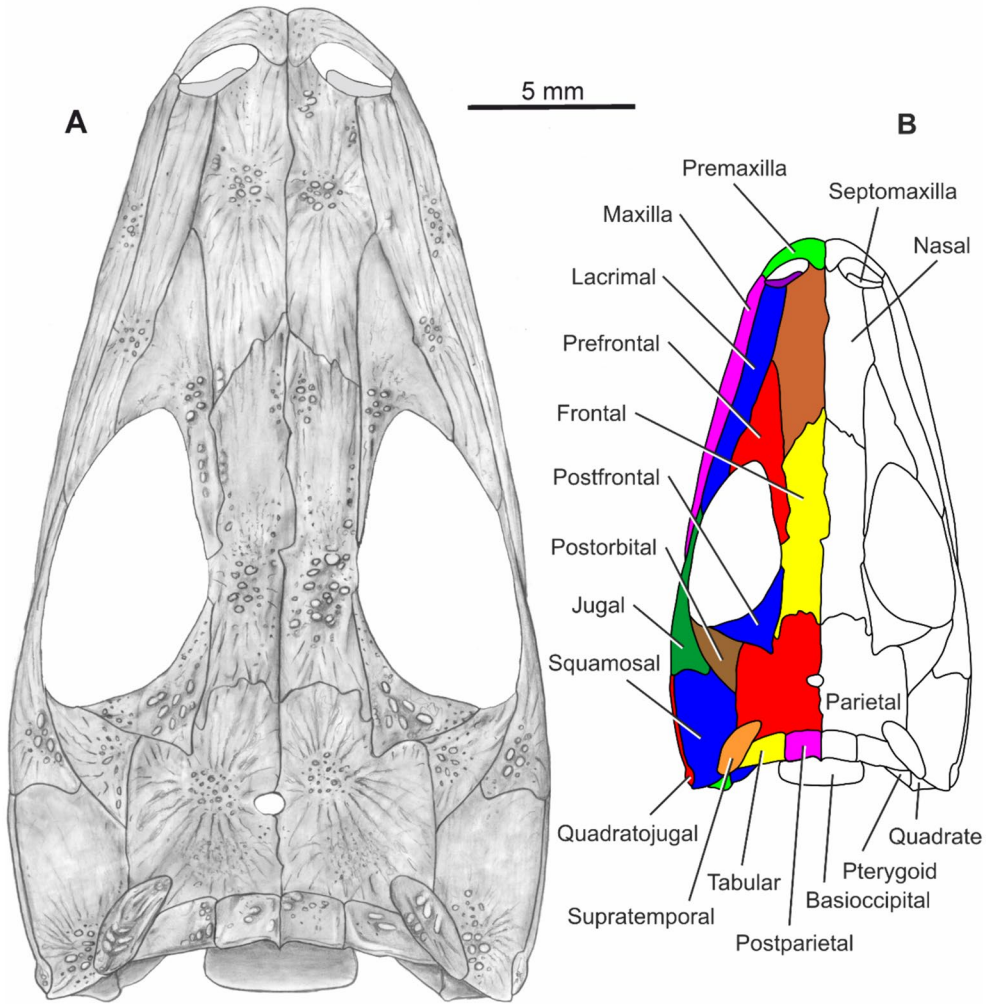

Fig. 13 *Brouffia orientalis* Carroll & Baird, 1972. **A** Skull reconstruction in dorsal view. **B** Colour-coded and labelled dorsal skull diagram

wedged between the posterolateral portions of the nasals. Part of the ventral surface of the left nasal, interpreted by Brough & Brough (1967) as a prevomer, forms a narrow strip of bone on the ventral side of the skull (Fig. 7), visible between the anteriormost extremities of the lower jaws. This strip of bone shows impressions of a tubercular sculpture. A similar sculpture has been observed on the ventral surface of the nasals in premetamorphic stages of the seymouriamorph tetrapod *Discosauriscus austriacus* (Klembara, 1997). Although only the posterior rami of both prefrontals are preserved (Figs. 1, 2, 5), the complete outline of the expanded anterior portion of the left prefrontal and a small section of the anterior portion of the right prefrontal are traceable as impressions. The prefrontal has a triangular shape. Its long posterior ramus has a robust construction and terminates in a blunt posterior extremity, as shown on the right-hand side of the skull. This extremity is separated from the anterior ramus of the postfrontal by a small contribution of the frontal to the orbit margin. The posterior ramus of the prefrontal contributes to the anterodorsal margin of the orbit. The expanded anterior portion of the bone forms an isosceles triangle narrowly inserted between the nasal and the lacrimal and entering the anterior margin of the orbit. A short, but distinct posteroventral process, particularly visible on the left prefrontal, extends for a short distance ventral to the mid-height of the orbit.

The elongate, subrectangular frontals are complete (Figs. 1, 2, 5). They are slightly narrower than the nasals, with posterolaterally to anteromedially orientated anterior margins, and transversely orientated posterior margins. The configuration of the anterior margin was already noted by Brough & Brough (1967) in their drawing of the left frontal. The frontals contact each other along the anteriormost portions of their medial margins. Posterior to this level, they are slightly

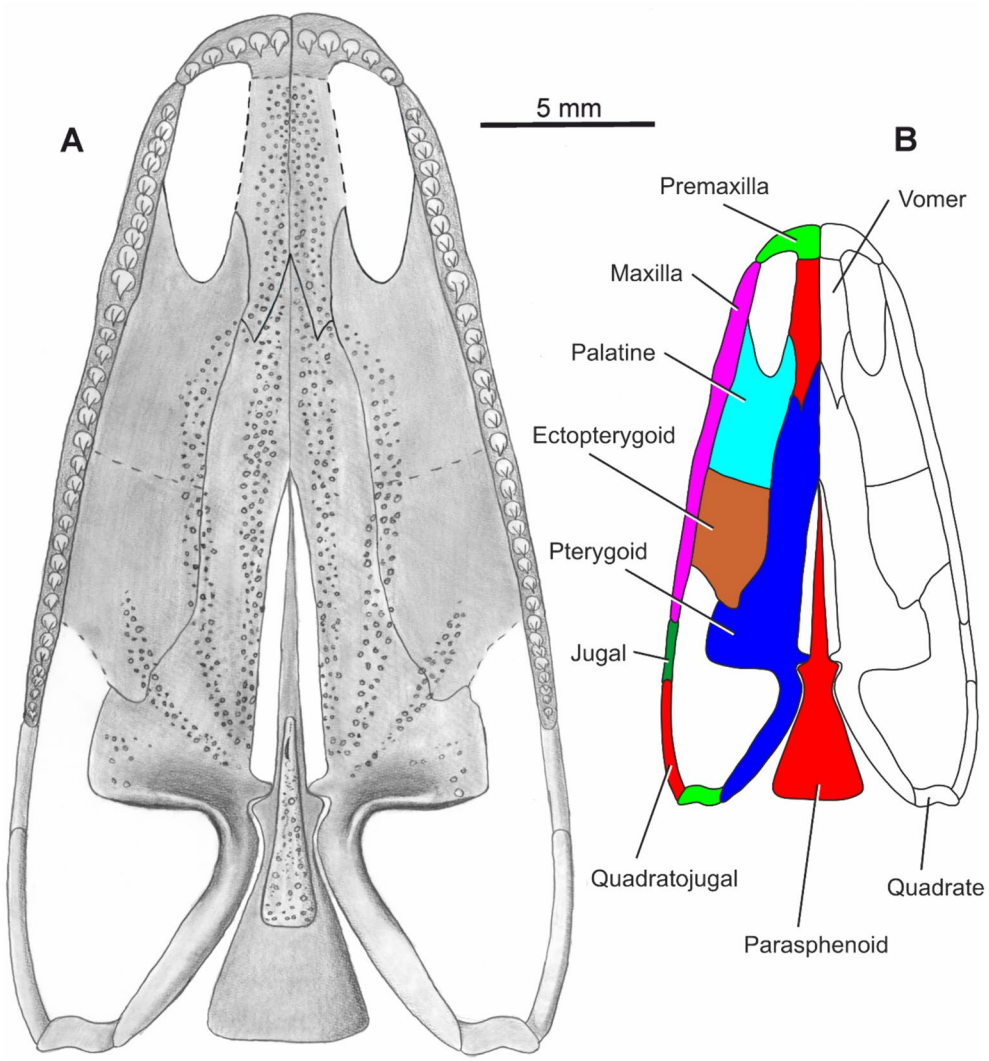

Fig. 14 *Brouffia orientalis* Carroll & Baird, 1972. **A** Skull reconstruction in ventral view. **B** Colour-coded and labelled ventral skull diagram

separated. Slightly posterior to its mid-point, the interfrontal suture presents a distinct inflexion, where the medial margin of the right frontal produces a small triangular process that fits into a small, embayed section along the medial margin of the left frontal. Similar inflexions observed in a variety of early tetrapods indicate that the process generally overlaps an underlying lamella (surface of bone overlap) associated with the recess (Klembara, 1997). The posterolateral corner of the frontal forms a gracile, digitiform process situated between the parietal and the postfrontal. This process extends posteriorly, reaching the level of the anterior one-third of the pre-pineal inter-parietal suture. It is accommodated by a small notch along the lateral margin of the parietal corpus (see below), a short distance anterior to the point where the parietal lappet merges into the parietal corpus. The frontal has a very short contribution to the dorsalmost part of the orbit margin, especially visible on the left-hand side of the skull.

Both postfrontals are represented, but only the left element appears complete and un-disrupted (Figs. 1, 2, 5). It is an approximately triangular bone that contributes to most of the posterodorsal margin of the orbit. A very short section of the smooth-surfaced and vertically orientated orbital wall is seen on the left postfrontal. The medial margin of the bone forms an extensive sutural contact with the frontal but only a short contact with the parietal. The suture between the lateroventral process of the postfrontal and the postorbital is approximately half as long as the latter bone. A slightly shorter sutural contact occurs between such process and the anterior margin of the parietal lappet. The postfrontal forms a small,

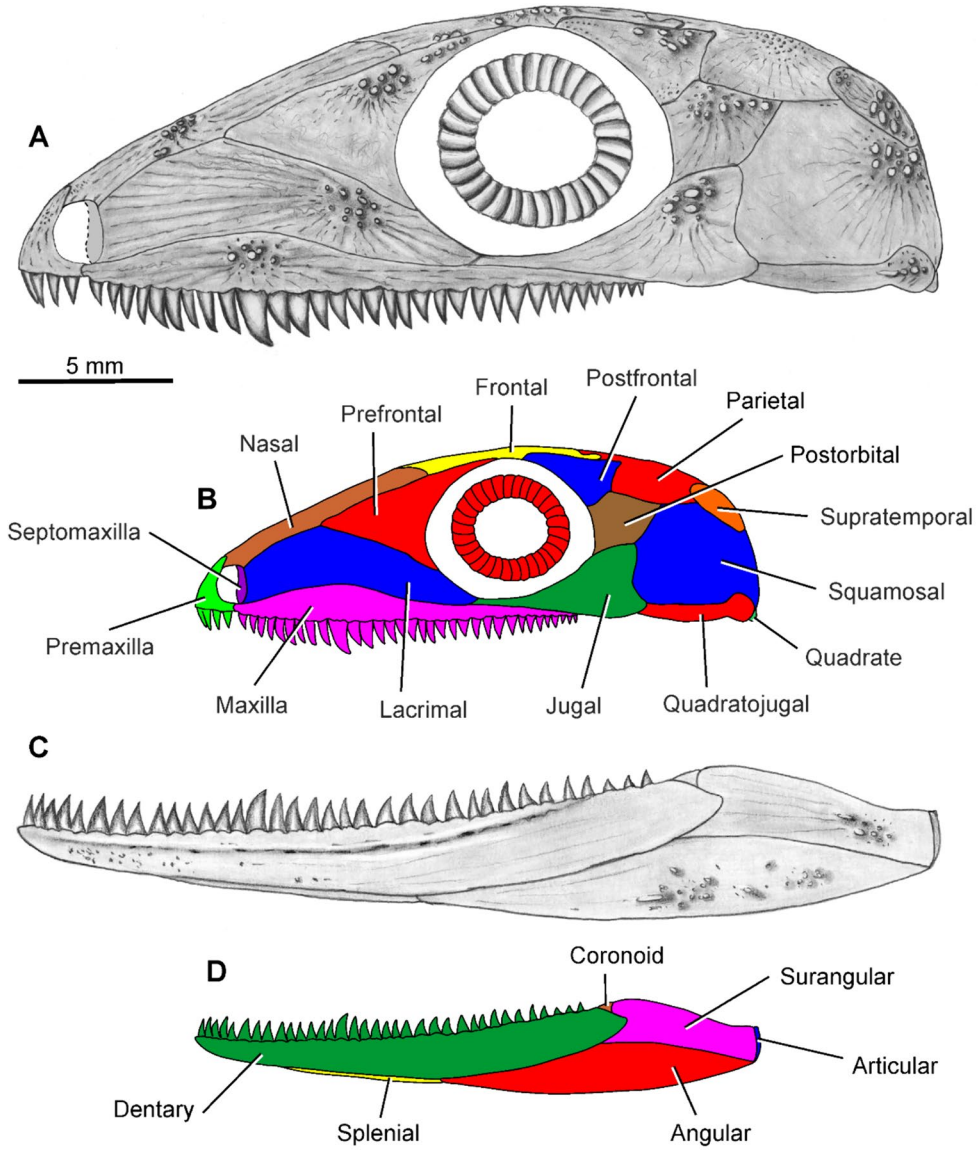

Fig. 15 *Brouffia orientalis* Carroll & Baird, 1972. **A** Skull reconstruction in left lateral view. **B** Colour-coded and labelled lateral skull diagram. **C** Reconstruction of left lower jaw in lateral view. **D** Colour-coded and labelled lateral jaw diagram

acuminate triangular projection at its posterior extremity, inserted between the parietal corpus and lappet.

The left parietal is nearly intact and well preserved (Figs. 1, 2, 5, 6). In contrast, the right parietal is damaged as the right pterygoid protrudes dorsally against its ventral surface. The entire medial sculptured surface of the right parietal is missing, and the sutural margins of its lateral portion cannot be observed (Figs. 5, 6). The parietal is divided into two elongate, subtrapezoidal portions: a medial corpus and a lateral lappet. The lappet is delimited from the corpus by an anteromedial and a posteromedial notch which accommodate, respectively, the posterior projection of the postfrontal and the anterior margin of the supratemporal. Although the parietal-frontal suture is scarcely visible, it appears to follow an irregularly interdigitating course, and occurs approximately at the same transverse level as the postfrontal mid-length. The slightly subelliptical parietal foramen is situated either at the same level as, or anterior to, the mid-length of the inter-parietal suture. The lappet forms a long suture with the postorbital and a marginally shorter suture with the squamosal. The triple sutural joint where the parietal, the postorbital, and the squamosal meet lies just posterior to the parietal foramen. Anterior to the foramen, the inter-parietal suture is nearly straight. Posterior to it, the suture is very gently sinuous. The posteriormost portion

of the parietal accommodates the tabular and postparietal (Fig. 6), as established by Carroll & Baird (1972). A slightly oblique ridge along the posterior margin of the left parietal marks the position of the sutural seam between the left parietal and the left tabular. Posterior to this ridge is a flat and slightly depressed area for the left tabular (Fig. 6). Most of its surface is smooth, except for its anteromedial portion which is covered in fine, anteroposteriorly orientated striations. Medial to this area is a second, slightly depressed area that underlapped the left postparietal. This area is smooth medially but covered in small, irregular tubercles laterally (Figs. 5, 6).

The left supratemporal is complete and preserved in situ (Figs. 1, 2, 5, 6), whereas the right supratemporal is slightly less complete and appears to have been displaced posteriorly, in a manner analogous to the displacement incurred by the two postparietals and by the right tabular (see below). The right supratemporal is marginally smaller and narrower than the left one, but this may be the result of preservation. The bone has an ellipsoid outline. Its greater axis is orientated anteromedially to posterolaterally. Its anterior one-third is accommodated by the posterolateral corner of the parietal. Its ossification centre occupies the posterior half of the bone.

The tabular has a subtrapezoidal outline (Figs. 1, 2, 5, 6). A bony element preserved just posterior to the left parietal almost certainly represents the left tabular. Its identification is based upon the fact that its outline matches that of the slightly depressed lateral articulation area along the posterior portion of the left parietal, described above. The right tabular is also preserved (Figs. 5, 6), but rotated by 90 degrees, such that its narrow lateral extremity faces anteriorly. The tabular narrows abruptly to a point laterally. Its dorsal surface bears distinct tubercles and ridges located mostly on its medial surface. The suture between the tabular and the postparietal is orientated anteroposteriorly. A smooth, strip-like occipital flange is visible posterior to the ornamented surface. The right tabular is smooth. For this reason, we speculate that its exposed surface might be ventral. According to Carroll & Baird (1972), the tabular is of similar shape to the supratemporal, but our findings suggest otherwise.

Both postparietals are complete and in articulation, and visible a short distance behind the parietals (Figs. 1, 2, 5, 6). They are rectangular and only marginally wider than long, and their posteromedial corners form acuminate posterior processes. Posterior to their sculptured surface is a smooth, narrow occipital flange. Whereas the posteromedial process is not shown in Brough & Brough's (1967) drawing of the skull, it does appear in Carroll's (1970) as well as Carroll & Baird's (1972) drawings, but it does not appear in their skull reconstruction.

Both maxillae are exposed. The right maxilla is particularly well preserved, and only its anterior extremity is disrupted (Figs. 1, 2, 3, 4, 5, 7). Morphological details of the lateral surfaces of both elements are visible. Their medial surfaces are damaged or obliterated (Figs. 3, 4, 7). The anteriormost portion of each maxilla is dorsoventrally narrow. The bone deepens rapidly in a posterior direction, reaching its greatest depth about halfway along its length. From this point, it decreases gradually in depth towards its posterior extremity. In its posterior half, it exhibits two subparallel sulci (Figs. 1, 5). The lower sulcus is distinctly deeper than the upper sulcus and terminates at the posterior end of the maxilla. On its medial surface, the bone has a well-developed supradental shelf (Figs. 3, 4).

The lacrimal is a large, elongate bone (Figs. 1, 2, 5) extending from the anteroventral margin of the orbit to the external naris. The right lacrimal is almost completely preserved. Its lateroventral portion is partially overlapped by the right maxilla and its posteroventral process is concealed. On the left side of the skull, the maxilla covers the middle part of the lacrimal, but the anteriormost and posteriormost portions of the latter are exposed. If our interpretation is correct, the posteroventrally orientated process of the lacrimal (jugal process) appears as a posteriorly tapering, robust strut tucked between the left maxilla and the left prefrontal (Fig. 5). In their drawing of the right lacrimal, Brough & Brough (1967) illustrated a jugal process, but we are unable to confirm their observation. The lacrimal-prefrontal suture is sinuous and marginally longer than the lacrimal-nasal suture. The lacrimal attains its greatest depth at the level of its triple sutural joint with the nasal and the prefrontal. Anterior to this level, the bone narrows imperceptibly and forms a subrectangular bony sheet. Posterior to the sutural joint, it narrows slowly up to the orbit margin, then more rapidly ventral to the anteroventral section of the orbit margin.

Although both postorbitals are observed, only the left element provides useful data on the morphology of the bone and its relationships with neighbouring elements (Figs. 1, 2, 5, 6). The postorbital is subtriangular and forms the second smallest contribution to the margin of the orbit, after the frontal. The medial margin of the postorbital is sutured with the parietal lappet. The posterior extremity of the postorbital-parietal suture extends posterior to the mid-point of the lateral margin of the lappet. The lateroventral ramus of the postorbital narrows to a point. The postorbital-jugal suture is slightly longer than the postorbital-squamosal suture and its anterior extremity is situated slightly below the mid-height of the orbit in lateral view. The right postorbital features a well-preserved orbital margin with a slightly raised and sharp peripheral rim.

The jugals are vaguely cleaver-shaped in outline (Figs. 1, 2, 5, 6, 7) although in neither is the posteriormost portion fully preserved. The bone consists of a broad posterior corpus and a slender anterior process. Across the transition between these two regions, the jugal decreases rapidly in depth up to the mid-point of the orbit length. Anterior to this point, the process is of approximately constant thickness and contacts the lacrimal at a level between the anterior and middle one-thirds of the orbit's anteroposterior diameter. The orbital margin is thick and with a smooth texture. The posterior margin of the bone forms a markedly sinuous suture with the squamosal. The ventral margin of the corpus is gently convex and probably lay flush with the ventral margin of the posterior extremity of the maxilla.

The shape and proportions of the squamosals can be inferred with some confidence, in part based upon the shape of surrounding bones, although its anterior and ventral margins are disrupted (Figs. 1, 2, 5, 6). The dorsal margin is visible on the right squamosal. It displays a thick peripheral rim along its anterior and middle one-thirds, where it contacts the postorbital along an anteroventrally slanting suture as well as the parietal lappet along a nearly horizontal suture, respectively. In this region, the dorsal margin of the squamosal is gently arcuate (Fig. 5). The posterodorsal portion of the bone forms a shallow embayment for the supratemporal. At this level, the posterodorsal margin slants posteroventrally. The straight posterior margin is subvertical and bears a shallow groove, broadest towards its dorsal extremity and gradually narrowing ventrally (Fig. 5).

The complete right quadratojugal and the posterior portion of the left quadratojugal are visible (Figs. 1, 2, 5, 6, 7). The posterior, subcircular articulation part of the bone continues into a club-shaped, stout anterior process with a nearly straight dorsal margin and a gently convex ventral margin. The boundary between these two regions is represented by a small constriction. The process is deepest at its mid-length and becomes dorsoventrally narrower anteriorly and posteriorly, terminating in a blunt anterior extremity. Carroll & Baird (1972) figured the quadratojugal as a strap-shaped element with acuminate anterior and posterior extremities and attaining its greatest depth in its anterior one-fourth. We have not been able to find evidence in support of their interpretation. We suspect that the bony sliver that appears next to the right squamosal in their drawing is either part of the squamosal or a small chunk of matrix (Figs. 5, 6, 7).

Sclerotic ring

Several dorsal and ventral sclerotic plates occur as faint impressions in both orbits (Figs. 1, 2, 5). At least five plates are visible in the left orbit (Fig. 2) and nine in the right orbit (Figs. 1, 5). They appear as mediolaterally elongate and rectangular elements (Fig. 5), about half as wide as long, but with no obvious surface details.

Palate

Most of the palate surface is visible, except for its lateralmost portions which are partially overlapped by the lower jaws (Figs. 3, 4, 7). The left pterygoid is completely preserved (Fig. 7). The posterior half of the right pterygoid is also clearly visible. The posterior half of the palatal ramus of the pterygoid narrows gradually anteriorly. At this level, its lateral margin is sinuous, being gently convex anterior to the point where the ramus detaches from the corpus of the pterygoid and then broadly concave up to the level where the two palatal rami contact each other. Further anteriorly, the palatal ramus widens slightly, and its lateral margin becomes convex. This convexity occupies the anterior one-third of the lateral margin. More anteriorly, this margin becomes very gently concave. The anterior part of the palatal ramus is narrowly triangular and carries an elongate and acuminate anteromedial projection and a subtriangular and abbreviated anterolateral projection. Between these two projections is a broadly V-shaped notch that accommodates the posterior extremity of the vomer (Fig. 7). The square transverse flange is well developed and carries a robust transverse ridge along its posterior margin. The articulation socket has a subtriangular outline. Both quadrate rami are preserved. A strong arcuate ridge occurs on the anteroventral portion of the quadrate ramus, close to its lateral margin, and continues smoothly into the transverse ridge. The narrow and elongate interpterygoid vacuities extend for more than half of the length of the palatal rami.

Carroll & Baird (1972) did not identify a vomer in *Brouffia*. However, the left-hand side of the palate shows a narrow space between the anteriormost tip of the left pterygoid and an elongate, narrow bony plate visible immediately lateral to it (Figs. 3, 4, 7). This plate fits into the above-mentioned V-shaped notch of the palatal ramus. We identify this bony plate as the posterior portion of the left vomer. The anteriormost extremity of the vomer is extensively overlapped by the anterior portion of the right splenial (Fig. 7). However, small denticles present immediately anterior to the anteriormost portion of the right splenial provide an indication of the possible anterior extent of the right vomer (Figs. 3, 4, 7).

The left palatine is almost complete, although its posterolateral portion is overlapped by the lower jaw (Figs. 3, 4, 7). It is an elongate plate with two robust anterior processes. The lateral maxillary process is longer than the medial vomerine process. Between the processes is a wide notch representing the posterior margin of the

choana. Although only partly visible, the outline of the choana suggests that this opening was substantial and probably extended posteriorly close to the level of the posterior extremity of the vomers.

Carroll & Baird (1972) interpreted an elongate piece of bone overlying the transverse flange of the left pterygoid as a fragment of the ectopterygoid (Figs. 3, 4, 6, 8). Whereas we are unable to support or reject this interpretation, we think it is plausible. The fragment forms a slender strip of bone and carries two large teeth close to one of its extremities (presumably, anterior) and probably also small denticles.

The parasphenoid plate is completely preserved and exposed in ventral view (Figs. 3, 4, 7). It is vaguely flask-shaped and with a distinct constriction immediately posterior to the basipterygoid processes. It reaches its greatest width at its posterior margin. The cultriform process is a narrow, stiletto-like structure gradually narrowing to an acuminate tip anteriorly.

Palatoquadrate ossifications

The internal surfaces of both quadrates are exposed. The left element is slightly better preserved than its antimere (Figs. 3, 4, 7). A lateral and a medial ridge cross the surface of the quadrate, running in an anterodorsal direction from the condylar portion. The ridges converge gradually, but do not meet. Further anteriorly, they appear to diverge slightly. The internal surface of the quadrate consists of small tubercles and ridges probably representing unfinished bone. If so, these elements were probably not fully ossified. The condylar portion is well preserved on the left quadrate.

Neural endocranium

The supraoccipital is preserved in dorsal view (Figs. 1, 2, 5). It consists of large right and left plates of approximately quadrangular shape. The right plate is slightly damaged. Both plates are joined by an anteroposteriorly short, median bony bridge. The posterior margin of the bridge constitutes the dorsal margin of the foramen magnum. The basioccipital is well-preserved and visible posterior to the parasphenoid (Figs. 3, 4, 7). It is a quadrangular plate with its posterolateral margins slightly converging posteromedially. The ventral surface of the basioccipital bears two anteroposteriorly orientated ridges with slightly convex lateral edges. Only the basipterygoid processes of the basisphenoid are visible (Figs. 3, 4, 7). They are short, with their articular surfaces directed at an angle of about 45° relative to the longitudinal axis. Carroll & Baird (1972) described a bony element preserved lateral to the basioccipital as an exoccipital. The same element was interpreted by Brough & Brough (1967) as a stapes. We can neither confirm nor reject either identification, due to the rather poor preservation of the element in question (Fig. 7).

Lower jaw

Carroll & Baird (1972) provided diagrammatic sketches of both lower jaws as well as a reconstruction of the right ramus in lateral aspect. However, no description of the lower jaw was supplied. In contrast, Brough & Brough (1967) illustrated the rami but gave only a limited account of their morphology. Our description differs from Brough & Brough's (1967) in several respects and we have been able to amend many of their original observations. Both rami are appressed against the ventral surface of the skull and are largely exposed in lateral aspect (Figs. 3, 4, 7). Small portions of their medial aspect, including details of some constituent bones, are visible inside the orbits in dorsal view (Figs. 1, 2, 5). The left ramus is almost fully articulated whereas the right ramus is disrupted.

The dentary is long and slender and occupies a little over two-thirds of the jaw length (Figs. 3, 4, 7). The posterior extremities of both dentaries are discernible within the orbits in dorsal view (Figs. 1, 2, 5). The external surface of the dentary is covered in longitudinal sulci and grooves, the course of which is disrupted by a network of cracks. One of these grooves is slightly deeper than the others and its course can be followed along most of the length of the dentary. This groove is situated in the dorsal one-third of the bone's external surface and is of approximately constant width. Near the anterior extremity of the ramus, this groove widens slightly and becomes shallower, merging indistinctly into the surrounding bone surface. At its posterior extremity, the groove approaches the upper margin of the dentary. Slightly posterior to its mid-length, the dentary is deepest, as reported by Carroll & Baird (1972). The posterior extremity of the dentary tapers abruptly, such that the portion of the bone that extends behind the last tooth forms a stout and subequilateral triangle wedged into the anterior portion of the surangular.

The angular is spindle-shaped (Figs. 7, 8) and reaches its greatest depth at the level of the posterior extremity of the dentary. Its anterior half gradually narrows dorsoventrally in an anterior direction. As preserved, it is tightly tucked between the dentary and the splenial at the level of its acuminate extremity. The posterior half of the bone also becomes increasingly narrow dorsoventrally, albeit less gradually than the anterior half. The external surface of the posterior portion of the angular is sculptured. The sculpture, which is better observed on the right angular (Figs. 3, 4, 7, 8), features subcentral tubercles and abbreviated ridges alternating with grooves, the latter increasing in length posteriorly.

Both surangulars form subrectangular, elongate plates (Figs. 3, 4, 7, 8). Immediately dorsal to the posterior process of the dentary, the anterodorsal extremity of the surangular is visible as a blunt semicircular process in contact with the coronoid along a small subvertical suture, visible in lateral view. Ventral to the posterior process of the dentary, the surangular extends anteriorly forming a triangular, pointed projection wedged between the dentary and the angular. A short distance behind the surangular-coronoid suture, the surangular attains its greatest depth and forms a distinct crest. Immediately posterior to the crest, the dorsal margin of the bone slopes gently posteroventrally, following a slightly convex course. At its posterior end, the margin becomes gently concave.

The posterior portion of the left coronoid is visible inside the left orbit in dorsal aspect (Figs. 1, 2, 5) and part of its external surface is exposed in ventral view (Figs. 7, 8). The coronoid extends posterodorsally as a narrow, rod-like strut attached to a plate-like, anterior portion (Fig. 5). This morphology suggests that this bone corresponds to the posterior coronoid. The dorsomedial surface of this plate is covered in closely packed denticles. *Protorothyris archeri* is the only other 'protorothyridid' in which the internal surface of the lower jaw is known (Carroll & Baird, 1972; Clark & Carroll, 1973). The single coronoid of *Protorothyris* (Clark & Carroll, 1973) lacks denticles. Thus, although incomplete, the coronoid of *Brouffia* clearly differs from that of *Protorothyris* and resembles closely that of *Gephyrostegus* (Klembara et al., 2014). The total number of coronoids is unknown in *Brouffia*.

The splenial appears as a slender bony splinter that contributes to the ventral margin of the jaw ramus (Figs. 3, 4, 7). In external view, its anterior extremity is estimated to have reached the level of the 7th dentary tooth, whereas its posterior extremity occurs slightly posterior to the last tooth. In the right lower jaw, the splenial is dislodged from its anatomical position and its external surface is fully exposed (Fig. 7). Its middle section is overlapped by several pieces of matrix. It is a flat, narrow, and fusiform bone with a thick ventral margin, reaching its greatest depth about halfway along its length. From this point, the splenial tapers gently towards its anterior and posterior extremities. Its anterodorsal portion is occupied by a deep notch (Fig. 7). This notch resembles a similar structure in the splenial of *Discosauriscus austriacus* (Klembara, 1997) and, perhaps, *Karpinskiosaurus ultimus* (Klembara, 2011). In these two seymouriamorphs, the splenial contributes to the posteroventral margin of a medial excavation situated immediately posterior to the lower jaw symphysis.

Both prearticulars are visible in the part and counterpart slabs (Figs. 1, 2, 3, 4, 5, 7). The posterior portion of the bone is robust but appears to be only partly ossified. Its quadrangular posterior portion is separated by a narrow constriction from a dorsoventrally narrow, anterior bony strip. This strip deepens gradually anteriorly, building the medial wall of the adductor fossa. However, its full anterior extent cannot be determined (Fig. 7).

The articulars are substantial elements (Figs. 3, 4, 7). The left articular is preserved as an irregularly ovoid bony patch, visible immediately posterior to the posterior extremity of the lower jaw (Fig. 7). Its exposed, presumably ventral surface is unfinished, similar to the condition noted for the posterior extremity of the prearticular. If confirmed, this observation would corroborate Carroll & Baird's (1972) conclusion that the holotype of *Brouffia* is not a mature individual. The right articular is preserved as a subrectangular fragment occupied by a subcentral transverse ridge. Its anteromedial corner forms a slender process, tucked between the quadrate and the quadratojugal, that extends anteriorly. However, no other information is available.

Dentition

Most upper and lower marginal teeth are visible (Figs. 1, 2, 3, 4, 5, 7), albeit slightly compressed. The teeth are subconical with their tips inclined posteriorly in different degrees. At least four teeth are visible in the left premaxilla, and there is space for one possible additional tooth. They differ little in proportions and decrease uniformly in height towards the front and the back of both the maxilla and the dentary. Many of the maxillary teeth (Figs. 1, 2, 3, 4, 5, 7) are covered in fine lingual striations close to their crown tips and a sharp crest runs along their anterior edge (Fig. 9). We found no evidence of a basal enamel folding, including in the largest teeth. The large depression visible in the mid portion of several tooth crowns results from crushing. Twenty-seven teeth can be observed in the left maxilla, with space for approximately three additional teeth. However, the anterior end of the bone is not preserved so that an accurate count is not possible. A large "caniniform" tooth is present in the anterior one-third of the left maxilla (Figs. 7, 8), as opposed to two "canines", such as were reported by Carroll & Baird (1972). None of the teeth that occur just anterior and posterior to the caniniform tooth matches the size of the latter (Figs. 4, 7, 9A). Twenty-four teeth occur in the right maxilla. A further nine additional teeth may have been present, although, as in the case of the left maxilla, the anterior end of the bone is missing (Figs. 1, 2, 3, 4, 5, 7). Our estimate of the maxillary tooth number is higher than that given by

Carroll & Baird (1972) and closer to that of *Palaeothyris* (estimated 35 teeth; Carroll, 1969). The left dentary shows 28 teeth, with room for another seven (Figs. 1, 2, 3, 4, 5, 7). Twenty-five teeth are visible in the right dentary, plus space for another eight or nine, with an estimated count of 35.

Most of the ventral surface of the vomer is covered by small and densely arranged denticles (Figs. 3, 4, 7). The denticles situated along the medial margin of the choana appear to be smaller than those covering the medial surface of the vomer.

The ventral surface of the palatal ramus of the pterygoid shows three elongate fields covered in small and closely spaced denticles. These three fields are separated by wide smooth surfaces that radiate out from the basicranial articulation (Figs. 2, 4, 7). Within these fields, the denticles form diverging rows. The posterolateral surface of the transverse flange bears a shagreen of irregularly arranged denticles. An anteroposteriorly elongate denticle field is present on the ventral surface of the left palatine (Fig. 7), and a large part of the dorsomedial surface of the left coronoid (Fig. 5). The fragment of bone identified as a left ectopterygoid carries three large, tusk-like teeth in its anterior portion and, possibly, a set of small denticles (Figs. 7, 8).

Lastly, a triangular field of small denticles occupies the middle one-third of the parasphenoid (Fig. 7). This field is shaped like an isosceles triangle, terminating in a narrow, pointed anterior extremity that extends a short distance anterior to the basipterygoid processes, ~ 21% of the length of the cultriform process. The patch widens posteriorly, nearly reaching the mid-length of the parasphenoid plate, where its greatest width is ~ 60% of the width of the plate at the same transverse level.

Postcranial skeleton

As in the case of the skull, the postcranial skeleton has undergone considerable diagenetic compression (Figs. 10, 11). Several sections of the vertebral column are difficult to discern due to poor ossification, disarticulation of individual elements, and/or obstruction from overlying structures. The details of the ventral surface of the vertebrae are partly obscured by the impressions of gastralia, which are arranged in elongate rows running anteromedially to posterolaterally from the ventral midline. In addition to gastralia, there are impressions of minute, round bony elements that appear irregularly scattered on the dorsal surface of the skeleton. Carroll & Baird (1972) regarded these elements as dorsal scales, but we have not been able to confirm or reject this interpretation.

Vertebrae

Various elements of the atlas/axis complex can be seen immediately behind the skull, although the precise identification of each is problematic (Figs. 10, 11). Two small, triangular fragments posterior to the supraoccipital may represent the paired proatlases. Both sides of the atlas neural arch, together with its posteriorly directed spine, are visible. A poorly preserved, rectangular bony fragment underlying the left atlas neural arch may represent one of the atlas centra. The axis centrum is the first centrum visible on the ventral surface. It is recognizable because it is slightly longer than the following centra (Fig. 11). The axis arch is visible on the dorsal surface (Fig. 10). Subtle variation in the morphology and proportions of the arches can be gleaned from Fig. 10.

The largest pleurocentra are approximately 3 mm long (Figs. 10, 11). The neural arches are in place but are not suturally attached to the pleurocentra, nor are they fused along the ventral midline. Small, sliver-like intercentra are especially discernible in the mid-trunk and pelvic regions. As Carroll & Baird (1972) noted, the ventral lip of some pleurocentra is beveled, indicating that it would have accommodated a small intercentrum. There are 31 presacral vertebrae, including the atlas and axis. The sacral vertebrae are not very dissimilar from adjacent vertebrae, except for the presence of a larger articulation area for the rib head. Two sacral ribs are visible on the left side of the specimen in dorsal aspect, corroborating the occurrence of two sacral vertebrae, as noted by Brough & Brough (1967). In contrast, only a single sacral vertebra was identified by Carroll & Baird (1972). Only the first four caudal vertebrae are preserved on the slabs and these resemble the last thoracic vertebrae (Figs. 10, 11).

Ribs

The slender and double-headed ribs do not show expanded distal extremities (Figs. 10, 11). The distal extremities of the short, straight, and flattened cervical ribs appear gently rounded. These ribs are approximately twice the length of an adjacent centrum. Most of the thoracic ribs are long and curved and terminate in somewhat squared-off extremities. Their length (in the mid-trunk region) corresponds to that of four to five centra. The two rib heads merge indistinctly. The last eight pairs of thoracic ribs are considerably shorter than more anterior thoracic ribs and decrease rapidly in length towards the pelvic girdle, where they are reduced to slender and straight spurs. The articulation areas on both sacral ribs is surrounded by a slightly raised peripheral rim. The anterior sacral rib has a flared, trapezoidal, flattened distal end, a gently concave anterior margin, an almost straight

(except proximally) posterior margin, and a gently convex distal margin. The posterior rib has a rectangular profile and a comparatively less expanded distal end. Its anterior and posterior margins have similar proportions to those of the anterior sacral rib (Fig. 10). The caudal ribs appear short (although longer than the sacral ribs), sturdy, and sharply angled. They do not appear to be fused to the centra, although most occur close the latter. No obvious traces of chevrons could be detected.

Pectoral girdle

The well-developed pectoral girdle shows no fusion of its endochondral elements (Figs. 10, 11). The clavicle is long, flat, and gently curved. Its lightly sculptured and subelliptical blade is only slightly wider than the widest portion of the clavicular stem. The stem has subparallel margins and terminates dorsally in a blunt parabolic extremity. As far as we can tell, the clavicle is marginally longer than four anterior trunk centra. We concur with Carroll & Baird (1972) that the bony rod occurring lateral to the left clavicle may represent a cleithrum. It is incomplete and nearly straight as preserved. Its identification is uncertain as it is similar in width to the adjacent ribs. In dorsal view, it shows an elongate, narrow triangular depression, possibly representing a sutural surface for the scapular blade (assuming its correct identification).

The interclavicle consists of a long, slender stem (as is typical of primitive amniotes and several amniote-like groups), and a broad, diamond-shaped plate. The posterior extremity of the stem is concealed underneath a trunk centrum. The stem changes in width along its length. Its posterior half shows nearly straight margins and increases very slightly in width posteriorly. Its central section, as preserved, is narrowest. Its anterior half has gently concave lateral margins and widens gradually anteriorly, merging almost indistinctly with the plate. The plate is approximately twice as wide as long and attains its greatest width at the level of the transverse axis that connects its lateral subtriangular processes. Anterior to these processes, the plate has a broadly semicircular outline. Posterior to the processes, at the transition between the stem and the plate, the posterolateral margins of the plate converge strongly posteromedially and present an irregularly sigmoid course. The densely sculptured central portion of the plate consists of irregular, pebble-like, and densely packed tubercles generally decreasing in size peripherally. This sculpture extends a short distance posteriorly, occupying a central strip on the anterior half of the stem. It also extends onto the medial half of the lateral subtriangular processes and becomes less conspicuous in the lateral half of these processes where the tubercles tend to be small and produce a low and irregular relief. The anterior and anterolateral portions of the plate are either smooth or covered in light striations.

The scapula is flat and sturdy. Its dorsal and ventral margins are gently convex, the former being marginally shorter anteroposteriorly than the latter. Its anterior margin forms a smooth, rounded convexity (more pronounced on the left scapula) immediately ventral to the mid-height of the bone. Dorsal and ventral to this convexity, the anterior margin is straight or irregular sinuous. The posterior margin features a shallow embayment slightly dorsal to the mid-height of the scapula. Dorsal and ventral to this embayment, the profile of the margin is nearly straight. The coracoids are represented by flat, featureless, and poorly defined bony masses visible on either side of the interclavicular stem. It is not clear whether one or two coracoids are present (Fig. 10).

Forelimb

Both left and right humeri are preserved, the right one being the more complete of the two. At about 15.5 mm, its length matches that of approximately five thoracic centra. The shaft merges smoothly into the proximal and distal extremities of the bone. The shaft reaches its minimum width slightly proximal to the mid-point of the total humerus length. It has an asymmetric profile, its posterior margin being slightly shallower than its anterior margin. The right and left humeri show subtle proportional differences and these may not be solely due to preservation. Thus, the posterior margin of the shaft of the left humerus appears to be gently sigmoid where it transitions to the proximal extremity. In contrast, the posterior margin of the right humerus is straight at the same level. Distally, a reverse arrangement is observed: at the transition between the shaft and the distal extremity, the right humerus has a gently concave posterior margin while the left humerus is markedly sigmoid. The distal extremity is gently expanded and fan-shaped and distinctly wider than the proximal extremity, which exhibits an irregularly trapezoidal outline (Figs. 10, 11). The abbreviated entepicondyle forms a blunt and triangular projection. A large and proximodistally elongate entepicondylar foramen is present. In extensor view, the foramen reveals an asymmetrical, teardrop-shaped outline and lies very close to the posterior margin of the entepicondyle. At its proximal end, the foramen narrows rapidly to a point. At its distal end, it shows a blunt, rounded profile. In flexor view, the foramen appears as an indistinct, comparatively shorter, more distally placed subelliptical depression. The proximal and distal articulation surfaces of the humerus are orientated at an angle of 90° relative to one another, as in several early amniotes. Neither an ectepicondylar ridge nor a supinator process are present. The distal articulation surface is indistinct and does not show

obvious condylar projections or surfaces and was probably largely cartilaginous in life, though we cannot rule out a preservation artefact.

The radius and ulna are relatively simple and undifferentiated elements. The margins of the shaft are shallow and concave, and their proximal and distal extremities are subrectangular. The two bones are of comparable lengths, and roughly equivalent to the combined lengths of three mid-thoracic vertebral centra. The slightly more gracile of the two bones may represent the radius. The bone identified as an ulna has more flattened proximal and distal extremities.

Combined information from part and counterpart slabs provides a substantial amount of morphological detail for the right manus, which we therefore describe in great detail. We are confident about the number of phalanges on digits I–III, as these are fully articulated. On digit V, the first phalanx as well as the proximal portion of the second can be seen on both slabs. A partly preserved ungual is also visible (Fig. 11). The space between the preserved portion of the second phalanx and the remnant of the ungual is likely to have been occupied by the distal part of the second phalanx. As for digit IV, we have expressed uncertainty as to the number of phalanges. Three articulated phalanges are clearly visible in flexor view (Fig. 11). In extensor view (Fig. 10), the proximal two-thirds of the first phalanx can be seen, as well as the distal extremity of the penultimate phalanx in articulation with an ungual. When the extensor and flexor views of the manus are superimposed, the length of digit IV appears to be consistent with the occurrence of five phalanges.

The shape and proportions of the five metacarpals (Mc) are gleaned from combined observations of the part and counterpart slabs. Only McIII and IV are visible in extensor and flexor views (Figs. 10, 11), whereas McI and II are fully exposed in extensor view only and McV in flexor view only. The longest metacarpal, McIV, measures a little more than half of the length of the radius and ulna (Fig. 10). It is distinctly more robust than each of the other metacarpals and the width of its shaft (about halfway along the length of the bone) is slightly smaller than the width of its proximal and distal extremities. McI-III and V exhibit a slightly more pronounced 'waisting' along their shafts than McIV. Furthermore, McII-V are vaguely sigmoid in their overall shape. This feature is made apparent by the changing curvature of the anterior and posterior margins of those metacarpals proximodistally and by the fact that the peripheral rims of their extremities are inclined at different angles relative to the main axis of the bones (Figs. 10, 11). McI differs from the other metacarpals in that its anterior margin is markedly concave, while its posterior margin appears straight through most of its length. Its proximal extremity shows two distinct sections, recognizable by their differently orientated peripheral rims. The posterior section (articulated with the most anterior distal carpal; Fig. 11) shows a straight rim, whereas the anterior section forms a robust and smoothly convex process with an anteroventrally oblique rim. Where the two rims merge, they form an obtuse angle between them. In terms of their absolute lengths, the metacarpals are arranged in the following order: McI < McV < McII < McIII < McIV. Using McI as a reference, the lengths of McV and McII represent an increase of ~ 9.67% and ~ 13.06%, respectively, relative to the length of McI, while those of McIII and McIV are ~ 36.35% and ~ 37.8%, respectively. The proximal ends of adjacent metacarpals McII-V are tightly appressed and there is no evidence that this pattern is an artefact of preservation.

The phalanges reveal considerable morphological variation, both within and between digits (Figs. 10, 11). Combined information from both the extensor and flexor views indicates that in the first phalanx of each digit, the proximal extremity is slightly more expanded than the distal extremity. The difference in width between the two extremities is more apparent in digits II-V. In those digits, the proximal extremity is broadly spatulate or fan-shaped, with a nearly straight or very gently convex peripheral rim and a slightly asymmetrical profile. The distal extremity, in contrast, is subrectangular and only marginally wider than the minimum width of the shaft. The anterior and posterior margins of those phalanges are gently concave, but their profiles differ. Thus, on digits III and V, the posterior margin is more deeply arcuate than the anterior margin. The reverse situation characterizes the proximal phalanx of digit IV. On digit II, both margins of the proximal phalanx are gently concave and with a comparable curvature. The first phalanx of digit I is of nearly constant thickness and shows a more robust build than the proximal phalanges of digits II–V. Its proximal extremity is only ~ 20% broader than its distal extremity. Its anteroproximal corner is slightly protruding, while its anterodistal corner is abbreviated and bluntly round. Its anterior and posterior margins appear moderately concave in their proximal one-third. The penultimate phalanges of digits II and III also have a robust aspect (Fig. 10). That of digit II is squat and vaguely sigmoid, with a gently concavity in the middle one-third of its anterior margin and a similar, shallow concavity along the distal half of its posterior margin. Its proximal and distal extremities are, respectively, squarish and subtrapezoidal. The phalanx is slightly shorter than the more proximal element on the same digit. The penultimate phalanx of digit III is subrectangular, with a straight posterior margin, and a small concavity along the distal half of its anterior margin. It is slightly longer than the more proximal phalanx in the

same digit and its extremities are approximately rectangular, as preserved. Subtle morphological details of the other phalanges, particularly on digits III and IV, are best conveyed by the illustrations in Figs. 10 and 11.

The slender digits terminate in short, sturdy, and claw-like unguals, visible on digits I-IV in extensor view (Fig. 10). In flexor view (Fig. 11), only the tip of the ungual on digit V is visible. The rest of this ungual is partly concealed underneath the first and second phalanges of digit IV. As preserved, the unguals are about half the length of the next most distal phalanx (Fig. 10). They show an asymmetric profile, presumably indicating that they lie on the plane of mediolateral flattening. Their length (distance from their apex to their proximodorsal part, the latter approximately coinciding with the base of the extensor tubercle; see Mann et al., 2021) increases imperceptibly from the first to the third ungual, then decreases slightly from the third to the fourth. The unguals on digits I and II are robust, due to the occurrence of a well-developed flexor tubercle (proximoventral part of the ungual) forming a sturdy, gently convex eminence on the second ungual, but reduced to a small process on the first. Both the first and second ungual terminate in a thick, beak-like extremity. The third and fourth unguals are vaguely talon-shaped and feature smoothly curved dorsal (convex) and ventral (concave) margins, although their distal tips are not markedly hooked (e.g., see Mann et al., 2021). Only the tip of the fifth ungual is visible in flexor view (Fig. 11). Its curvature resembles that of the third and fourth unguals, as far as we can tell.

The construction of the manus in *Brouffia* has few analogues among early reptiles. In a quick literature survey, we identified some general similarities with the Early Permian captorhinid *Romeria prima* (see Clark & Carroll, 1973, fig. 10), e.g., in the shape and proportions of McI (although this shows a comparatively shorter shaft in *R. prima*), the robust aspect of the first phalanx of digit I (slightly longer than McI and with a narrower, more demarcated waist in *R. prima*), and the sturdy unguals on digits I and II (but with a less pronounced curvature of the distal extremity in *R. prima*). The functional and/or phylogenetic implications of these traits are presently uncertain (see main text for a brief consideration of the lifestyle of *Brouffia*). The well-ossified wrist shows no fewer than seven carpals. In flexor view (Fig. 11), three large proximal carpals may be identified as the radiale, intermedium, and ulnare. More distally, four smaller bones occur, but their exact spatial arrangement is unclear. In extensor view, a single large carpal, presumably the ulnare, and five smaller carpals are visible (Fig. 10). It is likely that the full complement of centrals and distal carpals is present, although in a slightly disrupted arrangement. The phalangeal count is probably 2-3-4-5?-3, the generalized condition for early amniotes.

Pelvic girdle

The pelvic girdle is disarticulated. Its constituent elements are unfused, presumably indicating immaturity (Figs. 10, 11). As in the case of the pectoral girdle, the individual pelvic elements are preserved as flat bony plates with little surface detail. The stout ilium carries a single, short, and sturdy rectangular process directed posteriorly. The neck of the ilium is robust, with a nearly straight anterior margin and a smoothly concave posterior margin and is inclined posteriorly at about 45°. Where the anterior margin of the neck terminates dorsally, it joins the dorsal margin of the posterior process at an obtuse angle. The acetabulum has an asymmetric, subparabolic profile with a longer and gently sigmoid anterior margin and a shorter and 'stepped' posterior margin. The ischium is a broad plate resembling a quarter of a crescent in outline. It is deepest at its anterior extremity, which terminates in a smoothly convex anterior margin. Its posterior extremity forms a blunt and subtriangular process. The pubis is a round plate, again without obvious surface features.

Hindlimb

The right hind-limb is almost complete, but exhibits little anatomical detail (Figs. 10, 11). The femur is 17 mm long, only slightly longer than the humerus but somewhat more robust through the shaft. The proximal articulation is flat and strap-shaped, and there is little indication of an intertrochanteric fossa on the ventral surface. A narrow adductor crest is discernible. It extends from the proximal articulation almost to the distal articulations. Little can be seen of the distal articulation surface. The posterior condylar prominence appears to be folded over to a small extent.

The tibia and fibula are both similar in size and of comparable length to the radius and ulna. The tibia has a much wider proximal extremity than the fibula, terminates in a narrower, slightly flared distal end, and exhibits a nearly straight anterior margin and a gently arcuate posterior margin, attaining its greatest curvature along its proximal half. The peripheral rim of the proximal extremity consists of a shorter anterior section and a longer posterior section at an obtuse angle relative to one another. The fibula is rod-shaped and shows a subrectangular proximal extremity and a slightly more expanded, spatulate distal extremity than the tibia. Its anterior margin has a similar curvature to that of the posterior margin of the tibia, except that its greatest curvature occurs distally. The posterior margin of the fibula is nearly straight.

Some anatomical details are available for the pes, permitting a slightly more complete description than in previous works. The remains of a few tarsals and the entire first digit are preserved on the slab where the specimen is orientated in dorsal view (Fig. 10). Two large tarsals, presumably astragalus and calcaneus, are present, one in articulation, the other in the form of a poorly ossified bony mass occurring some distance from the distal end of the tibia and visible on both part and counterpart (Figs. 10, 11). Based upon its proximity to the tibia, this bony mass may represent a remnant of the astragalus. Although poorly ossified, it has a roughly pentagonal shape. There is no indication that it originates from the fusion of multiple ossification centres. While the juvenile condition of *Brouffia* would lead us to expect sutures (or traces of sutures) to occur in the astragalus if the latter did indeed originate from multiple ossifications, its poor preservation and the precocious ossification of the tarsals and carpals relative to the rest of the skeleton suggest caution in drawing a conclusion either way.

Only the first pedal digit is preserved (Fig. 10). It is somewhat longer and more robust than the first digit of the manus and terminates in a stout and claw-shaped ungual. The digit proportions are notable in that they are very different from those of stem amniotes, such as *Gephyrostegus*, in which an extremely shortened first pedal digit is present (Brough & Brough, 1967).

Scales

The ventral surface of the vertebrae is obscured by impressions of numerous ventral scales (gastralia) (Fig. 12). The ventral scales are flat, subrectangular plates with thick lateral margins, and are arranged in posterolaterally orientated rows. According to Brough & Brough (1967), there are two types of scales. The first and larger type, described by them as being 'oat-shaped', includes scales that are approximately three times longer than wide and with a weakly pronounced ridge along one side. The second, smaller type of scales includes 'rhomboidal' elements, about four times longer than wide. These two types of scales are not easily distinguishable, although we are able to confirm variation in size. The impressions of some scales, particularly in the middle portion of the trunk, suggest that some of the largest elements exhibited a much higher length:width ratio than that reported by Brough & Brough (1967). There appears to be little scale imbrication in both anteroposterior and mediolateral directions. We have not been able to confirm Brough & Brough's (1967) observation that the ribs cover the scales on both part and counterpart slabs, which would suggest the presence of a complete dermal armor.

Skull and lower jaw reconstructions

We present a new reconstruction of the skull of *Brouffia orientalis* in dorsal (Fig. 13), ventral (Fig. 14), and lateral views (Fig. 15A, B) and of the lower jaw in lateral view (Figs. 15C, D). In dorsal aspect, the skull is broadly parabolic, and the anterior margin of the snout is gently curved (Fig. 13A). As reconstructed, its length (measured from the anterior extremity of the conjoined premaxillae to a transverse line joining the rearmost projections of the squamosals) is slightly more than twice its width (greatest distance between the jugals). The nostrils are large and transversely elongate, and their distance is slightly less than half of the mediolateral nostril width. The anteroposterior diameter of the orbit is a little over 30% of the total skull length. The orbit centres are situated slightly posterior to the skull mid-length. The distance between the posterior margins of the orbits and the rearmost projections of the squamosals is approximately 73% of the distance between the anterior margins of the orbits and the snout. The width of the skull table (the greatest distance between the lateral margins of the parietal lappets) is a little over 57% of the total skull width.

Aside from overall skull proportions, our reconstruction (Fig. 13A) differs in several aspects of bone morphology from Carroll & Baird's (1972). Details of the antorbital region of the skull are scanty or non-existent in Carroll & Baird's (1972) reconstruction and, therefore, meaningful comparisons are not possible. In Carroll & Baird (1972), the anteromedial corner of the tabular projects slightly anterior to the anterolateral corner of the postparietal, whereas in our reconstruction the anterior margins of these two bones occur approximately at the same transverse level, except for the lateralmost tract of the anterior margin of the tabular. They are also slightly wider than long, and the postparietal is mediolaterally marginally narrower than the tabular (Figs. 1, 2, 5, 13A) and with a small, spur-like posteromedial process. The parietal lappet appears indistinct anteromedially in Carroll & Baird (1972), who illustrated the suture between the lappet and the posteromedial part of the postfrontal as being smoothly curved. In our reconstruction, the posteromedial corner of the postfrontal is narrowly triangular and sits in a deep incision of the parietal, which marks the transition between the corpus and lappet of that bone. Crucially, Carroll & Baird (1972) did not recognize the slender, long, and finger-like posterolateral process of the frontal that separates the anterolateral margin of the parietal corpus from the medial margin of the postfrontal. In Carroll & Baird (1972), the morphology of the frontal, postfrontal, and parietal on the right-hand side of the skull differs from that on the left-hand side. However, the right parietal is heavily disrupted, and we have not

been able to discern its precise shape and contacts with neighbouring elements (Figs. 1, 2, 5). For this reason, we have opted for a conservative approach in our reconstruction, such that the spatial arrangement of bones on the right-hand side of the skull mirrors that of their antimeres (Fig. 13A).

In lateral view (Fig. 15A), the skull is deepest slightly posterior to the mid-length of the orbit, as also shown by Carroll & Baird (1972). However, the course of sutures between the jugal, squamosal, and quadratojugal differs substantially between their reconstruction and our own. The dorsal and ventral corners of the posterior portion of the jugal are smoothly round and delimit a gently embayed posterior margin (Figs. 5, 15A). Carrol & Baird (1972, fig. 6A) also showed this margin in their drawing of the posterior portion of the left jugal. However, in their reconstruction of the skull in lateral aspect (Carrol & Baird, 1972, fig. 7D), the jugal features a slightly convex posterior margin. Our reconstruction also features a slenderer and strap-shaped quadratojugal than that figured in Carroll & Baird (1972) as well as a less deep squamosal and a more extensive postfrontal (Fig. 15A).

In ventral view (Fig. 14A), the pterygoids dominate the palatal surface. Together with the parasphenoid, they are the best-preserved bones of the palate. Most of the left palatine is also discernible, including the denticles covering its surface. Although the ectopterygoids are not preserved, their proportions may be estimated from the morphology of the surrounding bones. The posteroventral portions of the premaxillae are not preserved. For this reason, the lengths of their vomerine processes are only hypothetical. Our reconstruction does not differ in any substantive way from Carroll & Baird's (1972). The interpterygoid vacuities are comparatively narrower in our reconstruction and taper to a lesser degree anteriorly. Their length (from the medial ends of the basipterygoid processes to the posterior extremity of the inter-pterygoid suture) is approximately half of the distance from the basipterygoid processes to the anterior extremity of the inter-pterygoid suture. The choanae are proportionally wider and show a more gently curved posterior margin than in Carroll & Baird (1972).

The left lower jaw is reconstructed in external view (Fig. 15C). It is dorsoventrally slender and appears slightly more gracile than in Carroll & Baird's (1972) reconstruction. A detailed comparison between their reconstruction and our own is necessarily limited, in that they showed the posterodorsal portion of the lower jaw covered by the corresponding portion of the cheek in lateral view. Lastly, although the splenial is fully visible in internal view, the length of its exposure on the external surface of the lower jaw is only estimated (Fig. 15C).

Results

Phylogenetic analyses

Brouffia orientalis could be coded for 204 of the 295 characters in Klembara et al.'s (2023) amended version of Ford & Benson's (2020) data matrix. Fourteen characters were scored as inapplicable and another 77 as missing. A maximum parsimony analysis employing equally weighted characters resulted in nine shortest trees at 1615 steps (ensemble consistency index CI 0.2279; ensemble retention index R.I.=0.5876). Their strict consensus is shown in Fig. 16A. Protorothyridids form a polyphyletic array in all trees. *Brouffia* and *Coelostegus* emerge as sister taxa and form the sister group to Synapsida sensu Ford & Benson (2020). All other protorothyridid genera are nested between Captorhinidae and a diverse clade consisting of Araeoscelidia, Varanopidae, and Neoreptilia (i.e., Parareptilia plus Neodiapsida; Ford & Benson, 2020; Klembara et al., 2023). However, the interrelationships of these genera differ across the most parsimonious trees. In six of the trees, *Anthracodromeus*, *Hylonomus*, *Paleothyris*, and *Protorothyris* form a clade, either with (*Anthracodromeus*+*Hylonomus*) as sister group to (*Paleothyris*+*Protorothyris*) (two trees) or with *Hylonomus* and *Anthracodromeus* placed as successive sister taxa, in that order, to (*Paleothyris*+*Protorothyris*) (four trees). In three trees, the (*Paleothyris*+*Protorothyris*) clade, *Anthracodromeus*, and *Hylonomus* form a paraphyletic array relative to (Araeoscelidia+(Varanopidae+Neoreptilia)). Character resampling under both bootstrapping and jackknifing yielded support>50% for 23 nodes only across the entire phylogeny and, of those, only ten received support>70%. All protorothyridids were collapsed in both resampling procedures.

We carried out an additional parsimony analysis with equally weighted characters to explore in greater detail suboptimal tree topologies, especially with regard to the relationship between *Brouffia* and *Coelostegus*. To this end, we searched for the shortest trees that were not compatible with the (*Coelostegus*+*Brouffia*) clade. PAUP* produced 18 trees (length=1616; CI 0.2277; R.I.=0.5873), the strict consensus of which is illustrated in Fig. 16B. In these trees, *Brouffia* is the earliest diverging stem-group reptile, while *Coelostegus* appears as the sister taxon to Captorhinidae. The remaining protorothyridids genera are collapsed in a tetrachotomy consisting of *Anthracodromeus*, *Hylonomus*, (*Protorothyris*+*Paleothyris*), and all other reptiles.

A single tree (Fig. 16C) was obtained after re-weighting the characters by the largest values of their rescaled consistency indices from the previous analysis (length=213.31837; CI 0.3986; R.I.=0.7118). Protorothyridids are crownward of Captorhinidae and emerge as a paraphyletic group relative to Araeoscelidia-Varanopidae-Neoreptilia. In addition,

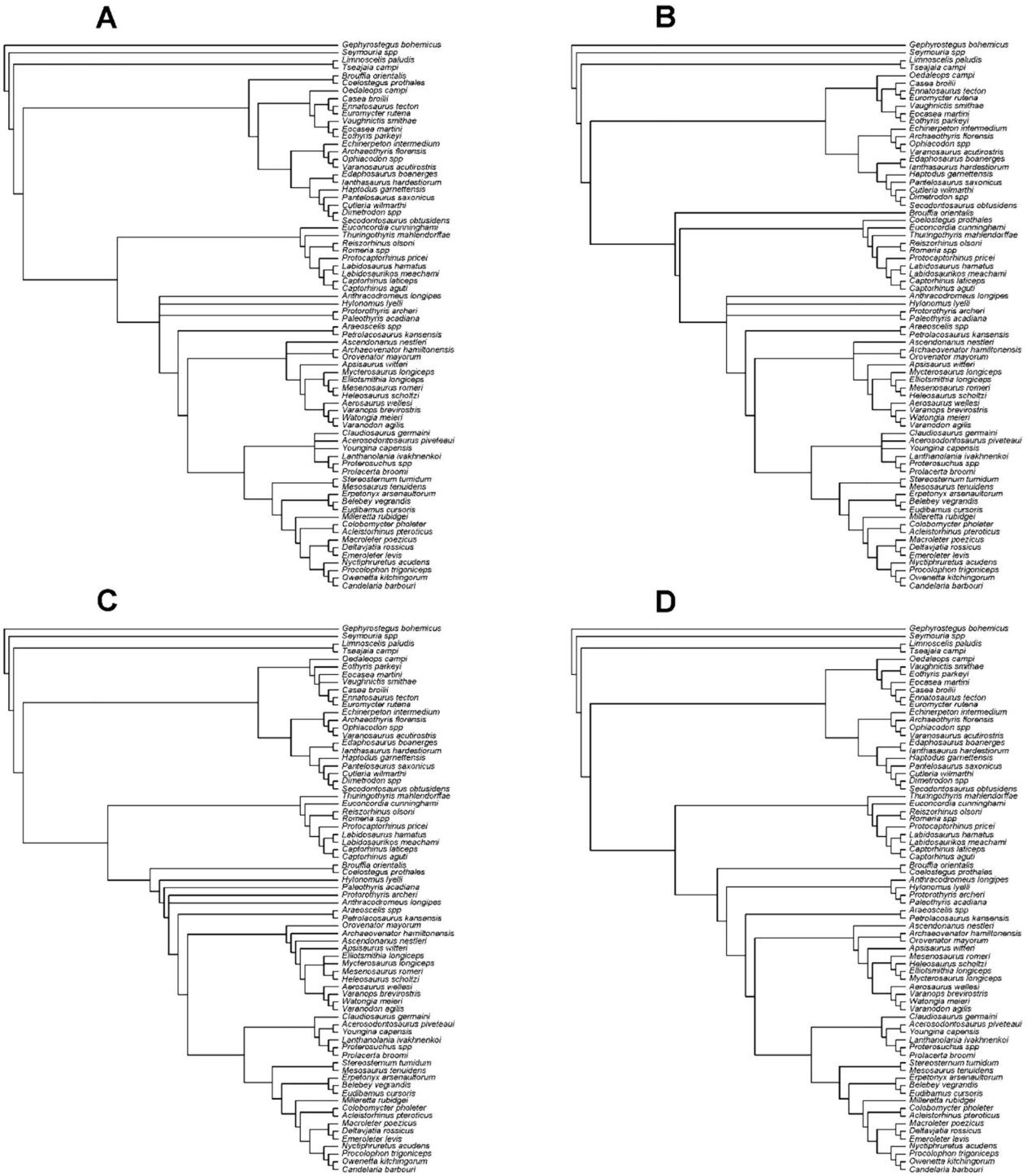

Fig. 16 Interrelationships of *Brouffia orientalis* Carroll & Baird, 1972. **A** Strict consensus of the nine most parsimonious trees from analysis with equally weighted characters (unit weight) and without topological constraints. **B** Strict consensus of the 18 most parsimonious trees from analysis with equally weighted characters, but not compatible with (*Coelostegus* + *Brouffia*) enforced as a topological constraint. **C** Single most parsimonious tree from analysis with all characters re-weighted by the maximum value of their rescaled consistency indices from **A**. **D** Single most parsimonious tree from analysis with implied weights

this latter clade is collapsed in a trichotomy along with *Protorothyris* and *Anthracodromeus*. The remaining protorothyridids, namely (*Coelostegus* + *Brouffia*), *Hylonomus*, and *Paleothyris*, form successively more crownward taxa, in that order, relative to this trichotomy.

Similar results were found with implied weights. The single tree (Fig. 16D; length = 1618; Goloboff fit = − 230.37883; CI 0.2274; R. I. = 0.5866) is fully resolved and differs from the tree obtained from simple re-weighting in the relative positions of some taxa within Synapsida and Varanopidae. Once again, protorothyridids are paraphyletic, with a clade of (*Coelostegus* + *Brouffia*) and a clade of (*Anthracodromeus* + (*Hylonomus* + (*Paleothyris* + *Protorothyris*))) as successive sister groups, in that order, to the Araeoscelidia-Varanopidae-Neoreptilia clade.

In the 50% majority-rule consensus of all sampled trees from the FBD analysis (Fig. 17), (*Coelostegus* + *Brouffia*) branches from the reptile stem-group anticrownward of Captorhinidae. The rest of the tree matches Ford & Benson's tree (2020). Crownward of Captorhinidae, *Hylonomus* and (*Anthracodromeus* + (*Paleothyris* + *Protorothyris*)) form a paraphyletic array relative to Araeoscelidia-Varanopidae-Neoreptilia. Reptilia—augmented through inclusion of *Brouffia* and *Coelostegus*—is weakly supported, with posterior probability (hereafter, p.p.) of 0.5681. The sister group relationship between *Brouffia* and *Coelostegus* receives very strong support (p,p. = 0.9968). In contrast, the node subtending Captorhinidae and all more derived groups has a p.p. of 0.3331. Very low support is also given to the node that includes *Hylonomus* and more derived groups

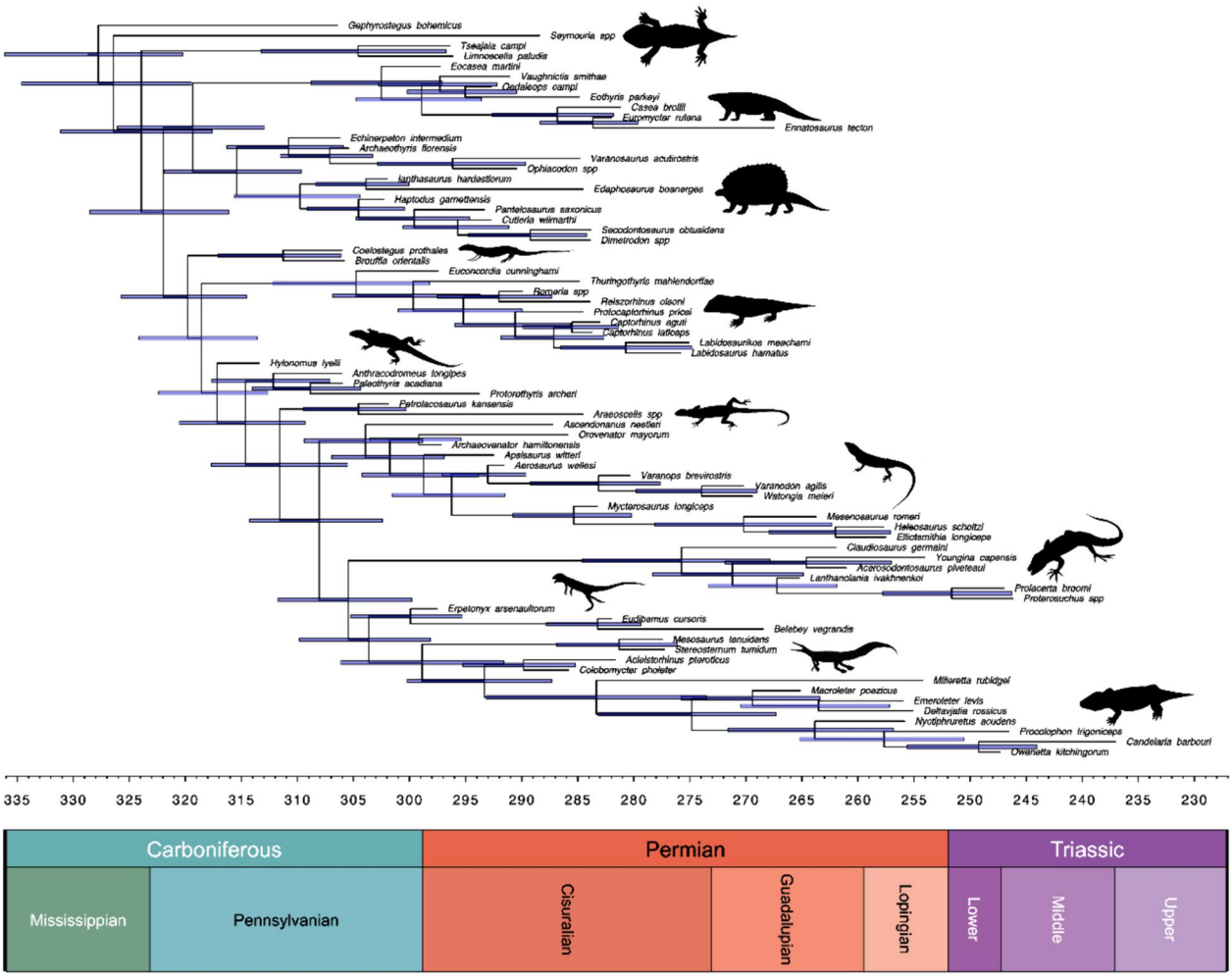

Fig. 17 Interrelationships of *Brouffia orientalis* Carroll & Baird, 1972. The Bayesian 50% majority-rule consensus (maximum clade credibility tree) from fossilized birth–death model. All groups compatible with the consensus are shown. The semi-transparent, purple horizontal bars represent 95% highest posterior density intervals bracketing the node ages

(p.p. = 0.3224), and to the internal nodes within the (*Anthracodromeus* + (*Paleothyris* + *Protorothyris*)) clade (p.p. = 0.2777 and 0.388). The node that links derived protorothyridids (*Anthracodromeus* + (*Paleothyris* + *Protorothyris*)) with the Araeoscelidia-Varanopidae-Neoreptilia clade is strongly supported (p.p. = 0.895). For a detailed account of other major branching events within Amniota and a discussion of node support, the reader is referred to Ford and Benson (2020).

The phylogenetic proximity of *Brouffia* and *Coelostegus*

Across all phylogenetic analyses, the close relationship between *Brouffia* and *Coelostegus* is supported by a host of homoplastic changes. For the equally weighted parsimony analysis, we arbitrarily selected the first of the nine most parsimonious trees to identify the character-state changes shared by those two taxa. For each character (character numbers in bold font follow the sequence in Ford & Benson, 2020), we report its consistency index, state transition (with single and double arrows representing ambiguous and unambiguous changes, respectively), and description of relevant state, in that order, under the accelerated transformation.

22, 0.375, 2 → 0: in lateral view, septomaxilla forming thin superficial bone bordering ventral margin of external naris (unknown in *Brouffia*; coded as uncertainty in *Coelostegus* along with alternative state 1 [rectangular sheet of bone shaped as a conical funnel]);
47, 0.250, 0 ⇒ 1: external naris position close to midline;
66, 0.154, 1 → 2: frontal posterolateral process long, narrow, frontoparietal suture forming acute posterolateral angle with parasagittal plane, substantially or fully separating parietal from dorsomedial margin of postfrontal;
111, 0.167, 0 ⇒ 1: postparietal (single or conjoined) width less than width of one parietal at its widest point;
128, 0.250, 0 → 1: parabasisphenoid body narrow, length greater than width (unknown in *Coelostegus*);
130, 0.286, 0 → 2: ventral surface of parabasisphenoid flat (unknown in *Coelostegus*);
164, 0.182, 0 ⇒ 2: mandible very long and dorsoventrally slender, with maximum height < 0.18 of total length;
185, 0.143, 1 → 0: presence of splenial exposure on lateral surface of mandible (unknown in *Coelostegus*);
190, 0.333, 0 → 3: ridge or keel absent from ventral surface of angular (unknown in *Coelostegus*);
197, 0.500, 0 → 1: surangular anterodorsal process dorsoventrally broad posteriorly and tapering anteriorly (unknown in *Coelostegus*);
206, 0.200, 0 → 1: cervical centra markedly longer than dorsal centra (unknown in *Coelostegus*);
217, 0.500, 0 → 1: posterior dorsal neural spines moderately anterodorsally inclined (state shown by *Coelostegus*, but alternative state 2 [strongly posterodorsally inclined] in *Brouffia*);
241, 0.250, 0 ⇒ 1: scapula anterior margin convex along entire length;
247, 0.400, 0 → 2: humerus radial condyle indistinct from ectepicondyle and entepicondyle (unknown in *Coelostegus*; likely ontogeny-related, but see Ford & Benson, 2020);
253, 0.214, 0 → 3: humerus supinator process very low or absent (unknown in *Coelostegus*; likely ontogeny-related, but see Ford & Benson, 2020);
258, 0.133, 2 → 0: ulna olecranon process absent or very low (unknown in *Coelostegus*; likely ontogeny-related, but see Ford & Benson, 2020);
261, 0.143, 0 → 1: transverse width across carpus at widest point (excluding pisiform) less than McIV (unknown in *Coelostegus*);
263, 0.143, 0 → 1: McIV length to radius length ratio > 45% (unknown in *Coelostegus*);
265, 0.250, 0 → 1: height to width ratio of manus unguals high, > 1.5 (unknown in *Coelostegus*);
277, 0.111, 0 → 1: femur length to humerus length ratio < 1.2 (unknown in *Coelostegus*).

Thirteen of the character-state changes listed above (47, 111, 128, 130, 185, 190, 206, 217, 241, 247, 258, 265, 277) also support *Brouffia* and *Coelostegus* as sister taxa in the single tree from the implied weights analysis (Fig. 16D). In the same tree, additional support is provided by the following character-state changes:

24, 0.118, 0 → 1: maximum dorsoventral height of preorbital ascending process of maxilla relative to height of maxilla at anterior orbit margin between 1.5 and twice the height (state shown by *Coelostegus*, but alternative state 2 [greater than twice the height] in *Brouffia*);
37, 0.200, 0 → 1: presence of maxilla 'supracanine' buttress on medial surface (unknown in *Brouffia*);
123, 0.286, 0 → 1: laterally directed basipterygoid processes (unknown in *Coelostegus*);
139, 0.250, 0 → 1: deep anterior incision of anterior surface of palatine (unknown in *Coelostegus*);
145, 0.222, 0 → 1: median contact between pterygoids > 50% of their anteroposterior length (unknown in *Coelostegus*);
158, 0.250, 0 → 1: quadrate inclined anterodorsally by 10–55 degrees;

189, 0.200, 1 → 0: coronoid teeth present (unknown in *Coelostegus*);
236, 0.111, 0 → 1: interclavicle posterior stem with expansion (unknown in *Coelostegus*);
255, 0.143, 0 ⇒ 1: radius length to humerus length ratio 0.68 to 0.82 (unknown in *Coelostegus*);
273, 0.200, 2 → 0: absence of mediolateral expansion along dorsal surface of ilium (unknown in *Coelostegus*).

Finally, in the single tree from the simple character re-weighting procedure (Fig. 16C), the (*Brouffia* + *Coelostegus*) clade is supported by several of the characters retrieved in the other two analyses (24, 37, 47, 66, 111, 123, 128, 130, 139, 145, 185, 206, 217, 236, 241, 247, 255, 258, 265, 277) and by the following additional characters:

216, 0.333, 0 ⇒ 1: outline of anterior and middle dorsal neural spines in lateral view sub-rectangular;
233, 0.167, 1 → 0: long axis of clavicle ventromedial plate and clavicle shaft delimiting highly obtuse angle;
256, 0.143, 0 → 1: radius longer than or approximately of the same length as the ulna (unknown in *Coelostegus*);
271, 0.143, 1 → 0: ilium with weakly concave or flat medial surface (unknown in *Brouffia*).

Three of the characters that support the (*Brouffia* + *Coelostegus*) clade—either together or in various combinations across the parsimony analyses—include a state that may be regarded as being ontogeny-related. None of the characters in question (247, 253, 258) can be scored in *Coelostegus*, but their putative 'ontogenetic states' are observed in *Brouffia*. Ford & Benson (2020) discussed the distributions of the states in question across different extinct amniotes. From their analysis and review of the specimens that provided the basis for their coding, it is clear that those states do not denote immaturity in all instances (species or groups) in which they occur. However, since the only known specimens of *Brouffia* and *Coelostegus* have been considered to be immature individuals, we carried out an additional parsimony analysis using equally weighted characters, from which characters 247, 253, and 258 were removed. We found nine shortest trees, the strict consensus of which is nearly identical to that in Fig. 16A. The only difference is that *Hylonomus* and *Anthracodromeus* appear as sister taxa in this new analysis.

Comparisons

Comparisons with *Paleothyris acadiana*

As noted by Klembara et al. (2023), detailed comparisons among protorothyridids must await a full redescription of several taxa. However, it is useful to highlight salient features that have potential diagnostic value. This is particularly relevant in the case of *Paleothyris acadiana*, which is somewhat similar to *Brouffia*, albeit slightly smaller and seemingly fully ossified. According to Carroll & Baird (1972), the possibility that these taxa are congeneric cannot be ruled out, and several skeletal traits of *Brouffia* may be related to ontogeny. New and revised information on *Brouffia* has highlighted several key differences between this genus and *Paleothyris* that, we believe, add strength to the argument that they are truly distinct. Since we have not been able to examine original material of *Paleothyris*, our discussion relies solely upon a detailed survey of Carroll's (1969) description and illustrations of *Paleothyris*. For ease of exposition, the following comparisons highlight the morphological conditions observed in *Brouffia* first.

(1) The anterior margin of the frontal slants posterolaterally to anteromedially and has a slightly irregular course. In contrast, the frontal of *Paleothyris* shows an undulating anterior margin with a transverse (mediolateral) course (see also comments on *Coelostegus* in the next section).
(2) The frontal has a long, narrow posterolateral process, the posterior tip of which fits into a small, distinct notch in the parietal. The process in question is absent in *Paleothyris*.
(3) The parietal has a lateral lappet that is delimited from the parietal corpus. A lappet is not present in *Paleothyris*.
(4) The posteromedial process of the postfrontal is accommodated by a deeply incised notch situated between the parietal lappet and the parietal corpus, extending slightly posterior to the anterolateral corner of the parietal lappet. In *Paleothyris*, the postfrontal forms a wedge lodged between the parietal and the postorbital.
(5) The articulation region of the quadratojugal is shaped like a subcircular projection and is separated by a constriction from the rod-like anterior region, which decreases in depth towards its anterior extremity. The quadratojugal of *Paleothyris* is depicted as a subtriangular and elongate bony splinter that narrows gradually to an acuminate anterior end and is deepest at its posterior end.
(6) The anterior margin of the supratemporal extends anteriorly relative to the anterior margin

of the tabular. In the reconstructed skull of *Paleothyris*, the supratemporal and tabular occur at the same transverse level.

(7) The tabular is wider than the postparietal. In *Paleothyris*, the tabular appears much narrower than the postparietal.

(8) The palatal ramus of the pterygoid gradually narrows to a point anteriorly, so that the conjoined palatal rami are narrowly inserted between the posterior portions of the vomers. In the reconstructed skull of *Paleothyris*, the anterior extremities of the palatal rami are wide and with transverse anterior margins abutting against the posterior margins of the vomers. In specimen MCZ 3482 of *Paleothyris acadiana*, however, Carroll (1969, text-fig. 2) figures the right pterygoid as having an anteromedial, gradually tapering process of the palatal ramus, as well as rows of small denticles lining the medial margin of such ramus, thus mirroring the morphology of the pterygoid in *Brouffia*. However, Carroll's (1969) descriptive account of the pterygoid, including its sutural contacts, appear to us to be inadequate and do not allow us to draw any form conclusions as to the actual proportions of this element.

(9) Three denticle rows are visible on the ventral surface of the palate, radiating out in an anterior direction from the area of the basicranial articulation. Unlike *Brouffia*, *Paleothyris* exhibits two rows of denticles.

(10) The entire middle portion of the ventral surface of the parasphenoid is covered in a denticle shagreen which occupies a narrow, elongate triangular field with well delimited lateral and posterior margins. In *Paleothyris*, the distribution of the parasphenoid denticles is variable. According to Carroll (1969), the patterns of denticle distribution shows three salient features: (a) denticles confined to a narrow ridge that extends anteriorly from the level of the basipterygoid processes (in the type specimen); (b) single or double longitudinal row of larger teeth along the posterior half of the cultriform process and extending slightly posterior to the level of the basipterygoid processes; (c) more or less continuous patch of denticles in the area between the basipterygoid processes.

In addition to skull characters, some postcranial traits also differentiate *Brouffia* from *Paleothyris*, notably the morphology and proportions of fore- and hindlimb elements (where observations are possible). The femur, tibia, and fibula of *Brouffia* resemble slightly sturdier versions of their homologues in *Paleothyris*. The manus of *Brouffia* is markedly dissimilar to that of *Paleothyris*, including in the proportions of metacarpals, phalanges, and especially the unguals. The radius and ulna of *Brouffia* are more compact and exhibit a less curved profile than their homologues in *Paleothyris*. Lastly, the humerus of *Brouffia* has a comparatively shorter and thicker shaft and a less pronounced entepicondyle than that of *Paleothyris*, and lacks a distinct ectepicondylar ridge.

The characters described above suggest that, while similar in many respects, *Brouffia* and *Paleothyris* are sufficiently distinct and ought to be kept in different genera. Independent support for this conclusion comes from the results of various phylogenetic analyses, none of which retrieves a close relationship between *Brouffia* and *Paleothyris*.

Comparisons with *Coelostegus prothales*

Our re-analyses of *Brouffia* and *Coelostegus* allow us to provide a more inclusive account of differences between these genera than those expounded by Klembara et al., (2023). As in the previous section, we describe the morphological conditions of *Brouffia* first.

(1) Acutely triangular, much narrower posteromedial process of the postfrontal ending in more acuminate posterior apex. In *Coelostegus*, the process in question was described by Klembara et al. (2023) as a triangular, smoothly convex, and tongue-like lappet. At present, it is unclear whether this process has any phylogenetic utility, but different clades and grades of early amniotes display different morphological conditions, in terms of its overall proportions, size, and pattern of overlap with the parietal.

(2) Conjoined parietals less distinctly wider than long. In *Coelostegus*, the width of the conjoined parietals (i.e., greatest distance between their lateral margins) exceeds their length (from the anterior margin of the parietal corpus to the posterolateral corners of lappets), but only by a small percentage increase in the width:length ratio compared to *Brouffia*. However, other proportional differences in parietal construction can be observed. The pre-pineal part of the parietal corpus is subrectangular in *Brouffia*, but elongate trapezoidal in *Coelostegus*. The length:width ratio of the parietal lappet is distinctly greater in *Brouffia* than in *Coelostegus*. A proportionally longer post-pineal portion of the inter-parietal suture is seen in *Brouffia*, while the post-pineal portion of

the suture is shorter than the pre-pineal portion in *Coelostegus*.

(3) Posterior margin of parietal not deeply embayed. In *Brouffia*, the posterior margins of the conjoined parietals delimit a straight or perhaps very shallow concavity. *Coelostegus* has a strongly arcuate posterior margin that turns rapidly posterolaterally immediately lateral to the triple sutural joint between the parietal, the postparietal, and the tabular.

(4) Squamosal slightly longer than deep. In *Brouffia*, the squamosal does not extend considerably behind the posterior margin of the skull table. Only about 10% of the length of the bone occurs posterior to the posterior margin of the supratemporal. This percentage rises to over 40% in *Coelostegus*, in which the squamosal contributes to an elongate suspensorium.

(5) Prefrontal with long, robust posteromedial process. The prefrontal of *Brouffia* has a distinct posteromedial process that contributes to most of the anterodorsal portion of the orbit margin. The process forms a robust strut which, at least on the left prefrontal, diminishes little in witdth anteroposteriorly. In *Coelostegus*, the process is much broader and abbreviated and shaped like an irregular triangle.

(6) Frontal with shorter, finger-like posterolateral process. In *Brouffia*, the process is stubby and digitiform, and measures less than one quarter of the length of the postfrontal. The homologue of this process in *Coelostegus* is a posteriorly acuminate, stiletto-like projection, nearly half of the length of the postfrontal.

(7) Comparatively narrower nasals and frontals. The width:length ratio of each of these bones is lower in *Brouffia* than in *Coelostegus*, regardless of whether length measurements of the frontals include or exclude the posterolateral processes of these bones.

(8) Nasal-frontal suture oblique. The anteromedially to posterolaterally slanting nasal-frontal suture of *Brouffia* contrasts with the mediolaterally orientated suture of *Coelostegus*. An oblique suture is not unique to *Brouffia* and occurs also in *Protorothyris archeri* (Clark & Carroll, 1973). Along with the general proportions of the frontal, the oblique anterior margin of this bone readily differentiates *Brouffia* from most other prototothyridids.

(9) Pineal foramen only slightly wider than long. In *Brouffia*, the width:length ratio of the pineal foramen (~ 1.37) is slightly less than that of *Coelostegus* (~ 1.65).

(10) Parietal-frontal suture slightly anterior to posterior margin of orbit. In *Brouffia*, the parietal frontal suture projects only a short distance anterior to the posterior margin of the orbit (~ 10% of the anteroposterior orbit diameter). This distance is proportionally greater in *Coelostegus* (~ 30%).

(11) Anterior margin of supratemporal anterior to parietal-tabular suture. In *Brouffia*, the supratemporal bisects the posterolateral corner of the parietal and terminates anteriorly in front of the anterior margins of the postparietal and the tabular. Although the supratemporal of *Coelostegus* shows similar proportions, its length is comparable to, or marginally less than that of the tabular. Furthermore, the construction of the posterior area of the parietal results in the supratemporal occurring noticeably posterior to the posterior margin of that element.

(12) Lacrimal depth increasing from margin of orbit to sutural joint between lacrimal, nasal, and prefrontal. In lateral aspect, the lacrimal of *Brouffia* becomes increasingly deeper from its anteroventral contribution to the orbit margin to the level of the common sutural joint with the prefrontal and the nasal. In *Coelostegus*, the lacrimal is deepest immediately anterior to the orbit, where a small inflection of its dorsal margin is observed. Anterior to this level, it decreases imperceptibly in depth and the latter remains approximately constant in an anterior direction.

(13) Triple sutural joint between frontal, nasal, and prefrontal situated slightly anterior to anterior margin of orbit. The point where these three bones intersect is situated only a short distance in front of the anterior margin of the orbit in *Brouffia* but is noticeably anterior to it in *Coelostegus* (distance between triple sutural joint and orbit ~ 15% of anteroposterior orbit diameter).

(14) Larger number of maxillary teeth (~ 35 vs. ~ 24). Along with *Hylonomus lyelli* and *Paleothyris acadiana*, *Brouffia* features the highest tooth count of all protorothyridids as well as one of the highest counts among early reptiles. Despite incomplete preservation of its maxillary arcade, *Coelostegus* clearly exhibits a much lower maxillary count, as originally described by Carroll & Baird (1972) (see also Klembara et al., 2023).

(15) Single "caniniform" maxillary tooth vs. region of "caniniform" teeth. A single and distinctly enlarged tooth, approximately occupying the 10th position from the anterior end of the max-

illa, occurs in *Brouffia*. *Coelostegus* shows a range of slightly enlarged teeth.

(16) Prefrontal-lacrimal suture entering orbit margin ventral to mid-height of orbit. The point where the posteriormost extremity of the prefrontal-lacrimal suture becomes confluent with the orbit margin occurs below the center of the orbit in *Brouffia* (with the skull observed in lateral aspect) but is approximately aligned with it in *Coelostegus*.

(17) Tabular subtrapezoidal. The tabular of *Brouffia* has a geometrically more regular outline than that of *Coelostegus* and could be described as a right trapezium. In contrast, the tabular of *Coelostegus* has an acute triangular shape, with gently curved, oblique anterior and posterior margins that converge posterolaterally into an acuminate process.

(18) Postparietal slightly wider than long with small, acuminate posteromedial process. The postparietal of *Brouffia* has a squarish outline and its posteromedial corner is drawn into a small, triangular spur-like process. The postparietal of *Coelostegus* is distinctly wider than long, with an oblique lateral margin and no posteromedial process, and its outline resembles an inverted isosceles trapezium.

Comparisons with *Protorothyris archeri* and *P. morani*

The two species of *Protorothyris*, *P. archeri* and *P. morani* (Clark & Carroll, 1973), reveal subtle differences in their skull construction. Therefore, we consider traits of *Brouffia* that differentiate it from that genus first, before tackling dissimilarities at the species level.

(1) Postfrontal with elongate, subtriangular anterior process. The process forms most of the posterodorsal margin of the orbit in *Brouffia* and extends anteriorly almost to the level of the orbit mid-length. In *Protorothyris*, it is stout and extends only a short distance anterior to the posterior margin of the orbit.

(2) Posterior margin of parietal without markedly concave profile. The parietal shows a very gently arcuate, nearly transversely orientated posterior margin in *Brouffia*. In contrast, this margin is deeply concave and with a subparabolic profile in *Protorothyris*. This peculiar configuration is partly linked to the next character.

(3) Parietal without spike-like posteromedial projection. In *Protorothyris*, the strongly embayed posterior margin of the parietal produces a posteromedial acuminate process. The adjoining processes of the two parietals result in a posteriorly protruding 'peak' of the dermal skull roof surface. In contrast, the medial sections of the posterior margins of the parietals in *Brouffia* has a slightly anteriorly convex profile.

(4) Smaller contribution of frontal to orbit margin. A short tract of the lateral margin of the frontal of *Brouffia* contributes to ~ 11% of the dorsal margin of the orbit in *Brouffia*. This margin receives a more substantial contribution from the frontal (> 30%) in *Protorothyris*.

(5) Proportionally larger supratemporal. In *Brouffia*, the length of the supratemporal, (size of along its greater axis), exceeds the width of each of the tabular and postparietal. The supratemporal of *Protorothyris* is an inconspicuous bony sliver, and the distance between its anterior and posterior margins is less than the greatest transverse width of each of the tabular and postparietal.

(6) Jugal-squamosal suture posteriorly concave. The jugal of *Brouffia* shows a smooth posterior concavity. In contrast, that of *Protorothyris* is gently convex and forms a series of irregular interdigitations with the squamosal.

(7) Posteriormost portion of prefrontal-lacrimal suture not interdigitating. In *Brouffia*, the prefrontal-lacrimal suture has a gently sinuous course and forms a gentle, posterodorsally orientated concavity immediately in front of the orbit. In *Protorothyris*, this tract of the suture is irregular, and in some specimens, it produces a strong interlocking pattern.

(8) Absence of transverse row of teeth on pterygoid flange. In *Brouffia*, the pterygoid flange (for a discussion of this structure, recent review in Mann et al., 2023) shows a robust, slightly raised transverse ridge close to its posterior margin, but no teeth occur on this ridge, unlike in *Protorothyris*.

(9) Palatal ramus of pterygoid widening slightly at mid-length. Unlike in *Brouffia*, the palatal ramus of the pterygoid narrows gradually in an anterior direction in *Protorothyris* (but not in *P. morani*; see Clark & Carroll, 1973, figs. 7C, F).

(10) Posterior margin of parasphenoid plate straight. The spatulate parasphenoid plate of *Brouffia* terminates in a transverse posterior margin. In *Protorothyris*, this margin is drawn into a sturdy, broadly parabolic process.

The most obvious difference between *Brouffia* and *P. archeri* is the fact that the latter taxon features a strong interlocking mechanism in the posteriormost portion

of the lacrimal-prefrontal suture, whereby a vertically orientated, triangular process of the lacrimal fits into a recess of the prefrontal immediately anterior to the anteriormost section of the orbit margin. In *P. archeri*, both the upper margin of the maxilla and the lower margin of the dentary have a 'stepped' profile, whereas such margins are smoothly curved in *Brouffia*. The surangular of *P. archeri* has a more elongate anteroventral process than *Brouffia*. In addition, the dentary of *P. archeri* forms a lanceolate process posterior to the tooth arcade ending in an acuminate tip. In *Brouffia*, the lateral margin of the parietal lappet is approximately parasagittal. In contrast, this margin diverges slightly posterolaterally in *P. archeri*. Contributing to this construction is a robust posterolateral process of the parietal that clasps the supratemporal. It is noteworthy that no such process occurs in *P. morani*. *P. morani* resembles *Brouffia* in the shape and size of the lateral lappet of the parietal, including its nearly parasagittal lateral margin, as well as in the position of the supratemporal, the anterior margin of which lies anterior to the tabular and postparietal. However, the parietals of *P. morani* are anteroposteriorly abbreviated just in front of the posteromedial corners of the postfrontals. The parietal-frontal sutures have strong interdigitations in some of the figured specimens of *P. morani* (Clark & Carroll, 1973, fig. 7). Variation in these interdigitations makes it unclear whether the frontals exhibit posterolateral processes. However, if the lateralmost interdigitation of the parietal-frontal suture in some of the *P. morani* specimens does represent such a process, the latter differs somewhat from the finger-like process of *Brouffia*. Lastly, immediately anterior to the orbit, the prefrontal of *P. morani* shows a small posteroventrolateral lappet, but this is absent in *Brouffia*.

Comparisons with *Cephalerpeton ventriarmatum*

The most obvious difference between *Cephalerpeton* and *Brouffia* (see Mann et al., 2019) are the smaller number of upper and lower marginal teeth, as well as the larger upper teeth in the former. The posteriormost tract of the prefrontal-lacrimal suture of *Cephalerpeton* features a strong interdigitation, not observed in *Brouffia*. In *Cephalerpeton*, the nasals are much shorter than the frontals and the preorbital region of the skull is more abbreviated than in *Brouffia*. In *Cephalerpeton*, the suborbital process of the lacrimal tapers rapidly in its posterior half and forms a slender bar. In contrast, the suborbital process of *Brouffia* is much thicker and ends in a blunt posterior extremity. As reconstructed (Mann et al., 2019), the quadratojugal appears slightly deeper (compared to its length) in *Anthracodromeus* and does not possess a distinct posterior constriction in front of the articulation region, unlike in *Brouffia*. The denticles are distributed more irregularly on the palate of *Cephalerpeton* than on that of *Brouffia*, although Carroll & Baird (1972) reported that the vomer and palatine denticles occur in uniform rows, and those along the medial margin of the palatal ramus of the pterygoid and along an oblique, anterolateral strip radiating from the area of the basipterygoid articulation are slightly raised relative to the rest of the ventral surface of the ramus.

Comparisons with *Anthracodromeus longipes*

The skull of *Anthracodromeus* is incomplete and comparisons with *Brouffia* are limited (see also Klembara et al., 2023). However, some features of the posteriormost region of its skull table are sufficiently informative. As in other protorothyridids, the supratemporal is a small elliptical plate but, unlike in *Brouffia*, its anterior margin is aligned with the anterior margin of the tabular. *Anthracodromeus* differs from *Brouffia* in possessing a triangular tabular with a concave medial margin sutured with the postparietal, a transversely oblong postparietal, and a broadly convex posterior lappet of the conjoined parietals. In addition, the lateral lappet of the parietal is anteroposteriorly abbreviated and features an angular lateral margin where the parietal-postorbital and parietal-squamosal sutures converge. Furthermore, the pre-pineal part of the parietal corpus of *Anthracodromeus* is proportionally much wider and shorter than that of *Brouffia* (Carroll & Baird, 1972). Lastly, the squamosal of *Anthracodromeus* appears to be slightly deeper than long, and the quadratojugal forms a stout, subfalciform bony strip.

Comparisons with *Hylonomus lyelli*

Hylonomus is too incomplete to permit comprehensive comparisons with *Brouffia*. Pending a thorough re-examination, the following cranial features of *Hylonomus* may provisionally be used to differentiate it from *Brouffia*: (1) postparietals at least three times wider than long; (2) jugal with subrectangular corpus; (3) obtusely angular posteroventral margin of the orbit along junction between corpus and suborbital processo of the jugal; (4) tabular projecting in front of postparietal; (5) squamosal with posteroventrally oblique lower margin; (6) small denticles on transverse flange of pterygoid; (6) two maxillary canines; (7) acuminate post-dental process of dentary (Carroll, 1964).

Discussion

The relationships of *Brouffia* and the chronology of early amniote evolution

The results of various phylogenetic analyses reveal—somewhat unsurprisingly—the unstable position of

most protorothyridids. A similar outcome characterized the analyses performed by Müller & Reisz (2006), albeit with different topological arrangements for the relevant taxa. In our parsimony analyses using different character weighting schemes (Fig. 16A, C, D), as well as in our FBD analysis (Fig. 17), *Brouffia* and *Coelostegus* consistently emerge as sister taxa. The results of our FBD analysis show some similarities with those found by Müller & Reisz's (2006, fig. 3) Bayesian analyses. Thus, *Coelostegus* occupies a basal position along the stem-group of Reptilia, either as the sole, earliest diverging plesion, as in Müller & Reisz's (2006) topologies, or alongside *Brouffia*, as in our FBD tree. In both Müller & Reisz's (2006) study and our work, Captorhinidae appear as the second earliest diverging plesion along the reptile stem. A major difference between their study and our own relates to the position of *Brouffia*. Thus, Müller & Reisz (2006) consistently placed *Brouffia* and *Hylonomus* as sister taxa, with (*Brouffia* + *Hylonomus*) as sister group to the Captorhinidae. In contrast, no protorothyridid genus is found to be phylogenetically proximal to Captorhinidae in our FBD analysis, while *Hylonomus* branches from the reptile stem immediately crownward of that group.

As for the parsimony analyses, our tree topologies are not reconcilable with the 50% majority-rule consensus in Müller & Reisz (2006, fig. 2). Thus, we retrieve Captorhinidae as the most basal plesion on the reptile stem, regardless of the character weighting scheme used. The intrinsic relationships within that group remain mostly unchanged in our parsimony trees and differ only in the placement of *Thuringothyris* or *Euconcordia* as the basalmost taxon. As for the protorothyridids, no common branching patterns emerge, emphasizing once again the conflicting distributions of character conditions, uncertain character polarity, and amount of missing data in this and other amniote groups. It is noteworthy that in the suboptimal trees in which the sister taxon relationship between *Brouffia* and *Coelostegus* is not supported (one extra step relative to the shortest trees), *Brouffia* is the most plesiomorphic taxon within the Reptilia, while *Coelostegus* forms the sister taxon to Captorhinidae (Fig. 16B). These results mirror in part those of Müller & Reisz's (2006) Bayesian analyses, except that the positions of *Brouffia* and *Coelostegus* relative to other amniote groups are reversed.

The most unexpected result of our parsimony analyses is the sister group relationship between (*Brouffia* + *Coelostegus*) and Synapsida when equally weighted characters are used. Clearly, neither *Coelostegus* nor *Brouffia* appear to be plausible near-ancestor candidates for Synapsida. However, recent work on early amniote relationships has dramatically altered our understanding of the affinities and status of several groups (e.g., Ford & Benson, 2018, 2020; Simões et al., 2022). Morphological similarities between some of the early members of both Synapsida and Reptilia have often been noted. Given the general lack of stability in the most basal branches of Amniota, certain taxa are likely to undergo considerable reshuffling across the phylogeny as a result of alternative schemes of character coding, weighting, and ordering, taxon and/or character inclusion and exclusion, *inter alia*.

It is useful to provide a brief account of the chronology of the main branching events near the base of Reptilia, based upon the results of the FBD analysis. The separation between the (*Brouffia* + *Coelostegus*) clade and more derived groups is placed at ~ 319.8 million years ago (Ma), with the latest common ancestry between those genera dating to ~ 311.28 Ma. The node subtending Captorhinidae and more crownward taxa dates to ~ 318.56 Ma. *Hylonomus* and more derived groups are estimated to have diverged ~ 317.15 Ma. (*Anthracodromeus* + (*Paleothyris* + *Protorothyris*)) separated from Diapsida sensu Ford & Benson (2020) ~ 314.15 Ma. Lastly, the node subtending (*Anthracodromeus* + (*Paleothyris* + *Protorothyris*)) dates to ~ 312.15 Ma, while *Paleothyris* and *Protorothyris* diverged ~ 308.86 Ma. Outside Reptilia, the origin of Synapsida is estimated at ~ 319.33 Ma and that of crown-group Amniota at ~ 321.98 Ma. Lastly, the age estimate for the divergence of Amniota from their immediate sister group, the Diadectomorpha, is ~ 323.92 Ma. There are only minor discrepancies between the median age estimates in Ford & Benson (2020) and our own. In both studies, the nodes that subtend Synapsida and Reptilia are comparable in age but whereas Ford & Benson's (2020) estimates fall within the early part of the Bashkirian (Lower Pennsylvanian), our estimates are slightly more recent (middle Bashkirian). Similarly, the origin of crown-group Amniota is placed in the late Serpukhovian (Upper Mississippian) in Ford & Benson (2020), and early Bashkirian in our study. Lastly, Ford & Benson's (2020) proposed divergence between Diadectomorpha and Amniota is estimated to have occurred in the middle Serpukhovian, while our estimate is close to the Mississippian-Pennsylvanian boundary (see also Brocklehurst et al., 2022 for a recent discussion of the chronology of early branching events in amniote history).

Close to the roots of Amniota, many of our age estimates differ remarkably, and tend to be much lower, than those in Simões et al., (2022), with the exception of the nodes leading to Synapsida, the median value of which is close to that found by Ford & Benson (2020). The much younger age for the node subtending Reptilia (= Sauropsida) in Simões et al.'s (2022) study (middle Moscovian) is unsurprising, given that their analysis re-assigned some putative lineages of primitive reptiles, including Araeoscelidia and (*Protorothyris* + Captorhinidae), to the amniote

stem-group. This redistribution results in earlier estimates for the origin of some nodes than those in Ford & Benson's (2020) and the present study. Examples include crown-group Amniota (middle Serpukhovian), the separation of the (Araeoscelidia + (*Protorothyris* + Captorhinidae)) clade from crown-group Amniota (earliest Serpukhovian), and divergence of the Amniota *s.l.*, i.e., ((Araeoscelidia + (*Protorothyris* + Captorhinidae)) + crown-group Amniota) from Diadectomorpha (middle/late Viséan). Obviously, these discrepancies necessitate an in-depth scrutiny of the phylogenetic placement of several key taxa, including protorothyridids, and a consideration of the influence of outgroups (see also Ford & Benson, 2018).

Possible lifestyle of *Brouffia*

We discuss the lifestyle of *Brouffia* using the results of a Principal Component Analysis of manus measurements across the range of tetrapod groups examined by Fröbisch & Reisz (1999) and Mann et al. (2021). In the bivariate scatterplot delimited by the PC1 and PC2 axes, *Brouffia orientalis* plots out in proximity to a heterogeneous cluster of squamate and mammalian taxa, such as iguanians (*Anolis equestris*; *Basiliscus plumiforns*; *Iguana iguana*; *Petrosaurus thalassinus*), lacertids (*Lacerta oxycephala*), dermopterans (*Cynocephalus volans*), as well as megachiropterans (*Ptenochirus minor*; *Epomops franqueti*) (Fig. 18). As in Mann et al., (2021), the left-hand half of the plot, towards decreasing scores on PC1, is dominated by taxa exhibiting increasing proportional lengths of McIII. The smallest PC1 scores pertain to mid- and large-sized rodents capable of sustained cursorial (running; trotting; galloping) and swimming lifestyles. The top right-hand side quadrant of the plot features chamaeleons as well as some marsupials and primates, along with *Anthracodromeus*. Most taxa in this region of the plot feature arboreal (or presumed arboreal) habits, as described by Mann et al., (2021), and are characterized by the increasingly greater proportional length of the proximal phalanx (towards large positive scores on PC1 and PC2). In contrast, the bottom rigth-hand side quadrant is dominated by megachiropterans and dermopterans, one lacertid, some iguanians, and the protorothyridid *Brouffia*. These taxa show moderate to high positive PC1 scores (albeit never attaining the largest PC1 values of chamaeleonids) and lowest PC2 scores and are characterized by the increasingly greater proportional length of the penultimate phalanx.

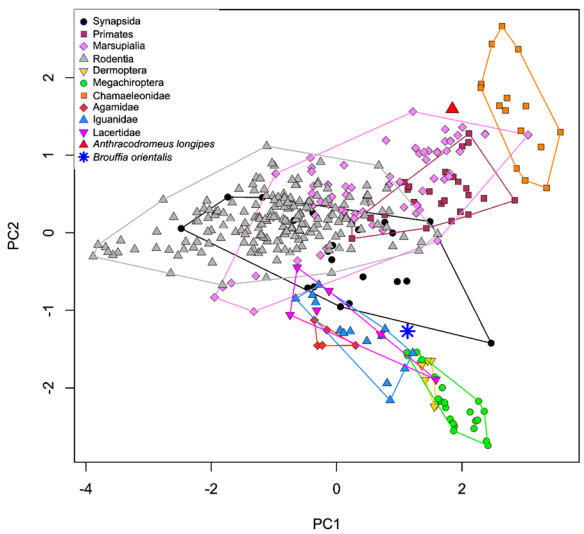

Fig. 18 Bivariate scatterplot of 367 tetrapod specimens in the plane delimited by the first two PC axes, based upon a Principal Component Analysis of manus proportions using the dataset in Fröbisch & Reisz (1999) and Mann et al., (2021). Colour codes for groups match those in Mann et al., (2021). Groups are delimited by convex hulls. The red triangle and blue asterisk mark the positions of *Anthracodromeus longipes* and *Brouffia orientalis*, respectively

A global test of the differences between the average Euclidean distances of *Brouffia* from the ten taxonomic groups in Fröbisch & Reisz (1999) and Mann et al., (2021) returns a significant result (Kruskal–Wallis chi-squared = 168.39, df = 9, p-value < 2.2e−16), with post-hoc tests producing 31 significant pairwise group comparisons. A depiction of group-specific distributions of taxon-taxon distances is shown in Fig. 19. The average distance of *Brouffia* from dermopterans is significantly lower than its average distances from most other groups (except iguanians and lacertids) (Supplementary Information, Additional file 4).

The manus of *Brouffia* differs from that of *Anthracodromeus* (Mann et al., 2021) in four respects. First, it is comparatively more robust and less elongate. Second, it possesses a proportionally shorter proximal phalanx and a longer penultimate phalanx of digit III. Third, the unguals (at least on digits I and II) are sturdier and less strongly hooked distally. Fourth, the proximal extremities of adjacent metacarpals are closely appressed. As Fig. 18 shows, *Brouffia* plots out close to a range of taxa with manifest arboreal-clinging adaptations. Obviously, clinging abilities such as are observed in the colugos (dermopterans) and fruit bats (megachiropterans), let alone their gliding and flying adaptations, are difficult to envisage in *Brouffia* and are not supported by any skeletal specializations of its wrist, ankle, and vertebral column. However, all squamates that occur proximal to *Brouffia* in the PC scatterplot demonstrate climbing adaptations and are habitually (e.g., *Anolis equestris*) or occasionally (e.g., *Lacerta oxycephala*) arboreal. The strong unguals of digits I and II appear superficially similar to the manus unguals in the basal anomodont synapsid *Suminia* and, as hypothesized for the latter, may have enabled adherence to tree surfaces

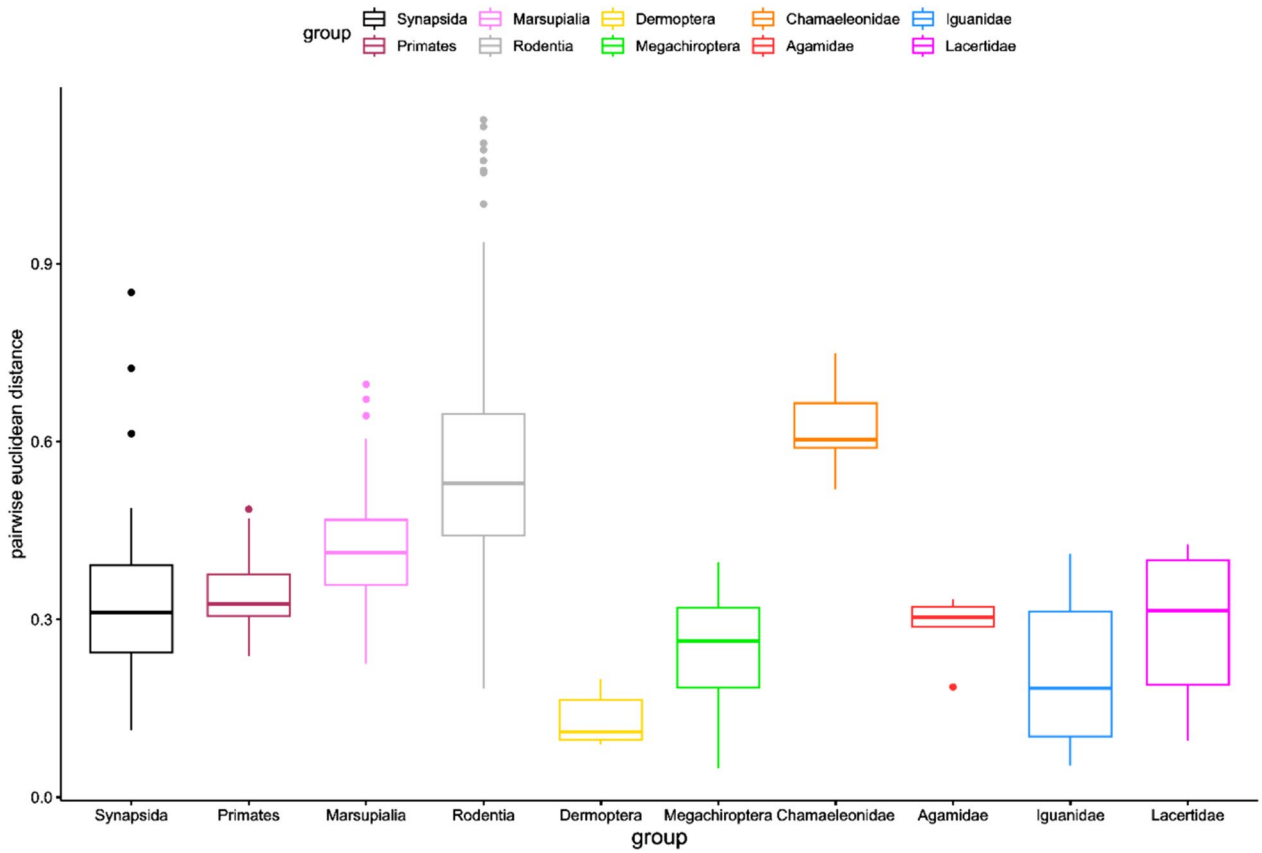

Fig. 19 Distribution of pairwise Euclidean distances between *Brouffia* and taxa in each of ten groups, using box-whisker plots. For each group, the colour-coded dots represent outliers (if present), the thin vertical line connects the minimum (lower) and maximum (upper) values of the distribution excluding outliers, the rectangular bar features the interquartile range (middle 50% of the value distribution), and the thick horizontal line is the median value

during climbing. There is no evidence that *Brouffia* had a prehensile manus, since McI is not divergent (i.e., orientated at an angle) from other metacarpals, and its proximal end contacts McII (see Fröbisch & Reisz, 1999 for a detailed discussion of these traits). However, the appressed proximal extremities of the metacarpals of *Brouffia*, while not forming a 'tight complex' like that of *Suminia*, do suggest a certain degree of rigidity within the autopod.

In conclusion, reliable inference for the lifestyle of *Brouffia* must await discovery of more complete specimens. However, the anatomy of *Brouffia* provides important data on the range of possible functional adaptations within early amniotes, prompting a consideration of niche differentiation and evolution of locomotor specializations in Carboniferous tetrapods.

Supplementary Information

The online version contains supplementary material available at https://doi.org/10.1186/s13358-024-00329-2.

Additional file 1. This document includes two sections. The first section is a compendium of photogrammetric 3D scanning techniques, based upon the protocols expounded in Klembara et al., (2023). The second section details the steps for conducting the morphometric analysis of manus proportions across the tetrapod dataset used by Fröbisch & Reisz (1999) and augmented by Mann et al., (2021) through the inclusion of *Anthracodromeus*.

Additional file 2. PAUP*-readable NEXUS file for conducting the parsimony analyses. This file was obtained by coding *Brouffia* in the taxon/character matrix of Klembara et al. (2023), a slightly modified version of the Ford & Benson (2020) matrix. For a list of characters, see Ford & Benson (2020).

Additional file 3. MrBayes-readable file for conducting the Bayesian fossilized birth/death analysis. This file was obtained by adding *Brouffia* and *Coelostegus* to the FBD script used by Ford & Benson (2020). The FBD settings were left unchanged.

Additional file 4. Tabulation of p-values for post-hoc comparisons of the pairwise differences between mean groupwise distances (see Fröbisch & Reisz, 1999 and Mann et al., 2021)

Acknowledgements
We are indebted to Dr Boris Ekrt (National Museum, Prague, Czech Republic) for granting us permission to study the specimen of *Brouffia orientalis* and for preparing two casts. The illustrations of the reconstructed skull and lower jaw (Figs. 13, 14, 15) were executed by Miriam Süllová (Bratislava, Slovakia).

Author contributions
JK, JA conceived the study. JK, MH, MR curated the data. JK, MR, TM, JA produced the formal analysis. JK, MH—funding acquisition. JK, MR, JA, TM investigated the specimen and produced the original draft. JK, DV, MR, MH—methodology. JK, MR, JA, TM wrote the original draft. JK, MR, JA reviewed and edited the manuscript. All authors read and approved the final version of the manuscript.

Funding
This project was supported by the Scientific Grant Agency of Ministry of Education of Slovak Republic and Slovak Academy of Sciences, Grant Number 1/0228/19 (to J.K.) and by Agency of Ministry of Education of Slovak Republic and Slovak Academy of Sciences, Grant/Award Number: APVV-22-0328 (to M.H.).

Data availability
All relevant data are in Supplementary Information.

Declarations

Competing interests
The authors declare no competing interests.

Received: 16 February 2024 Accepted: 11 July 2024
Published online: 11 September 2024

References

Brocklehurst, N., Ford, D. P., & Benson, R. B. J. (2022). Early origins of divergent patterns of morphological evolution on the mammal and reptile stem-lineages. *Systematic Biology, 71*, 1195–1209.
Brough, M. C., & Brough, J. (1967). The genus *Gephyrostegus*. *Philosophical Transactions of the Royal Society of London B, 252*, 147–165.
Carroll, R. L. (1964). The earliest reptiles. *Journal of Linnean Society (Zoology), 45*, 5–83.
Carroll, R. L. (1969). A Middle Pennsylvanian captorhinomorph, and the interrelationships of primitive reptiles. *Journal of Paleontology, 43*, 151–170.
Carroll, R. L. (1970). The ancestry of reptiles. *Philosophical Transactions of the Royal Society of London B, 257*, 267–308.
Carroll, R. L., & Baird, D. (1972). Carboniferous stem reptiles of the family Romeriidae. *Bulletin of Museum of Comparative Zoology, Harvard University, 143*, 321–363.
Clark, J., & Carroll, R. L. (1973). Romeriid reptiles from the Lower Permian. *Bulletin of Museum of Comparative Zoology, Harvard University, 144*, 353–407.
Farris, J. S., Albert, V. A., Källersjö, M., Lipscomb, D., & Kluge, A. G. (1996). Parsimony jackknifing outperforms neighbour-joining. *Cladistics, 1996*(12), 99–124.
Felsenstein, J. (1985). Confidence limits on phylogenies: an approach using the bootstrap. *Evolution, 39*, 783–791.
Ford, D. P., & Benson, R. B. (2018). A redescription of *Orovenator mayorum* (Sauropsida, Diapsida) using high-resolution µCT, and the consequences for early amniote phylogeny. *Papers in Palaeontology, 5*, 197–239.
Ford, D. P., & Benson, R. B. (2020). The phylogeny of early amniotes and the affinities of Parareptilia and Varanopidae. *Nature Ecology and Evolution, 4*, 57–65.
Fröbisch, J., & Reisz, R. R. (1999). The Late Permian herbivore *Suminia* and the early evolution of arboreality in terrestrial vertebrate ecosystems. *Proceedings of the Royal Society B, 276*, 3611–3618.
Gavryushkina, A., Welch, D., Stadler, T., & Drummond, A. J. (2014). Bayesian inference of sampled ancestor trees for epidemiology and fossil calibration. *PLoS Computational Biology, 10*(1003919), 1–15.
Goloboff, P. (1993). Estimating character weighting during tree search. *Cladistics, 9*, 83–91.
Goloboff, P., Torres, A., & Arias, S. (2018). Weighted parsimony outperforms other methods of phylogenetic inference under models appropriate for morphology. *Cladistics, 34*, 407–437.
Heath, T. A., Huelsenbeck, J. P., & Stadler, T. (2014). The fossilized birth-death process for coherent calibration of divergence-time estimates. *PNAS, 111*, E2957–E2966.
Jaekel, O. (1902). Ueber *Gephyrostegus bohemicus* n. g. n. sp. *Zeitschrift der Deutschen Geologischen Gesellschaft, 54*, 127–132.
Jaekel, O. (1909). Ueber die Klassen der Tetrapoden. *Zoologischer Anzeiger, 34*, 193–212.
Klembara, J. (1997). The cranial anatomy of *Discosauriscus* Kuhn, a seymouriamorph tetrapod from the Lower Permian of the Boskovice Furrow (Czech Republic). *Philosophical Transactions of the Royal Society of London B, 352*, 257–302.
Klembara, J. (2011). The cranial anatomy, ontogeny and relationships of *Karpinskiosaurus secundus* (Amalitzky) (Seymouriamorpha, Karpinskiosauridae) from the upper permian of the European Russia. *Zoological Journal of the Linnean Society, 161*, 184–212.
Klembara, J., Clack, J. A., Milner, A. R., & Ruta, M. (2014). Cranial anatomy, ontogeny and relationships of the Late Carboniferous tetrapod *Gephyrostegus bohemicus* Jaekel, 1902. *Journal of Vertebrate Paleontology, 34*, 774–792.
Klembara, J., Ruta, M., Anderson, J., Mayer, T., Hain, M., & Valaška, D. (2023). A review of *Coelostegus prothales* Carroll & Baird, 1972 from the Upper Carboniferous of the Czech Republic and the interrelationships of basal eureptiles. *PLoS ONE, 18*(e0291687), 1–31.
Laurenti, J. N. (1768). *Specimen Medicum, Exhibens Synopsin Reptilium Emendatam Cum Experimentis Circa Venena Et Antidota Reptilium Austriacorum*. Joan Thomae.
Mann, A., Dudgeon, T. W., Henrici, A. C., Berman, D. S., & Pierce, S. E. (2021). Digit and ungual morphology suggest adaptations for scansoriality in the late Carboniferous eureptile *Anthracodromeus longipes*. *Frontiers in Earth Science, 9*, 1–13.
Mann, A., McDaniel, E. J., McColville, E. R., & Maddin, H. C. (2019). *Carbonodraco lundi* gen et sp nov, the oldest parareptile, from Linton, Ohio, and new insights into the early radiation of reptiles. *Royal Society Open Science., 6*(191191), 1–15.
Mann, A., Pardo, J. D., & Sues, H. D. (2023). Osteology and phylogenetic position of the diminutive 'microsaur' *Odonterpeton triangulare* from the Pennsylvanian of Linton, Ohio, and major features of recumbirostran phylogeny. *Zoological Journal of the Linnean Society, 197*, 641–655.
Modesto, S. P., & Anderson, J. S. (2004). The phylogenetic definition of Reptilia. *Systematic Biology, 53*, 815–821.
Müller, J., & Reisz, R. R. (2006). The phylogeny of early eureptiles: comparing parsimony and Bayesian approaches in the investigation of a basal fossil clade. *Systematic Biology, 55*, 503–511.
Price, L. I. (1937). Two new cotylosaurs from the Permian of Texas. *Proceedings of the New England Zoölogical Club, 11*, 97–102.
Romer, A. S. (1952). Late Pennsylvanian and early Permian vertebrates of the Pittsburgh-West Virginia region. *Annals of Carnegie Museum, 33*, 47–113.
Ronquist, F., & Huelsenbeck, J. P. (2003). MRBAYES 3: Bayesian phylogenetic inference under mixed models. *Bioinformatics, 19*, 1572–1574.
Simões, T. R., Caldwell, M. W., & Pierce, S. E. (2020). Sphenodontian phylogeny and the impact of model choice in Bayesian morphological clock estimates of divergence times and evolutionary rates. *BMC Biology, 18*, 1–30.
Simões, T. R., Kammerer, C. F., Caldwell, M. W., & Pierce, S. E. (2022). Successive climate crises in the deep past drove the early evolution and radiation of reptiles. *Science Advances*. https://doi.org/10.1126/sciadv.abq1898
Stadler, T. (2010). Sampling-through-time in birth-death trees. *Journal of Theoretical Biology, 267*, 396–404.
Sumida, S. S., & Lombard, R. E. (1991). The atlas-axis complex in the late Paleozoic genus *Diadectes* and the characteristics of the atlas-axis complex across the amphibian to amniote transition. *Journal of Paleontology, 65*, 973–983.
Swofford, D. L. (1998). *PAUP∗ phylogenetic analysis using parsimony (∗and other methods) Version 4*. Sinauer Associates.
Tsuji, L. A., & Müller, J. (2009). Assembling the history of the Parareptilia: phylogeny, diversification, and a new definition of the clade. *Fossil Record, 12*, 71–81.
Zhang, C., Stadler, T., Klopfstein, S., Heath, T. A., & Ronquist, F. (2016). Total-evidence dating under the fossilized birth-death process. *Systematic Biology, 65*, 228–249.

Publisher's Note